magnetochemistry

MDPI

Article

Impact of the Different Molecular Weights of Polyethylene Glycol (PEG) Coating Agents on the Magnetic Targeting Characteristics of Functionalized Magnetoresponsive Nanoclusters

Sandor I. Bernad [1,2,*], Alexander Bunge [3,*], Maria C. Ioncica [2], Rodica Turcu [3], Monica Dan [3], Vlad Socoliuc [1], Daniela Susan-Resiga [1,4] and Elena S. Bernad [5]

[1] Centre for Fundamental and Advanced Technical Research, Romanian Academy—Timisoara Branch, Mihai Viteazul Str. 24, RO-300223 Timisoara, Romania; vsocoliuc@gmail.com (V.S.); daniela.resiga@gmail.com (D.S.-R.)
[2] Research Center for Engineering of Systems with Complex Fluids, Politehnica University Timisoara, Mihai Viteazul Str. 1, RO-300222 Timisoara, Romania; cristina.ioncica@gmail.com
[3] National Institute for Research and Development of Isotopic and Molecular Technologies (INCDTIM), Donat Str. 67-103, RO-400293 Cluj-Napoca, Romania; rodica.turcu@itim-cj.ro (R.T.); monica.dan@itim-cj.ro (M.D.)
[4] Faculty of Physics, West University of Timisoara, Vasile Parvan Str. 4, RO-300223 Timisoara, Romania
[5] Department of Obstetrics and Gynecology, University of Medicine and Pharmacy "Victor Babes" Timisoara, P-ta Eftimie Murgu 2, RO-300041 Timisoara, Romania; ebernad@yahoo.com
* Correspondence: sandor.bernad@upt.ro (S.I.B.); alexande_b@gmx.de (A.B.)

Abstract: In this article, we investigated the influence of molecular weight (Mw) on particle deposition efficiency after PEG-functionalized (polyethylene glycol-PEG) magnetoresponsive magnetic cluster targeting. In this work, the clusters were obtained by the solvothermal polyol method using polyethylene glycol (PEG) as a coating agent. So, we investigated three kinds of magnetoresponsive clusters: MNC-2000, MNC-6000, and MNC-10,000. These clusters were coated with PEG, and had molecular weights (Mw) of 2000 Da, 6000 Da, and 10,000 Da, respectively. The authors propose that the key to achieving maximum efficiency in targeted drug delivery is to deposit a thin, uniform layer of medication that covers the vascular wall in the area of interest. We defined a set of efficiency criteria to focus on the most essential characteristics of the targeting results. These are the obstruction degree, which measures the level of vessel obstruction; the magnet coverage degree, which evaluates the quality of particle deposition along the vessel wall; and the proximal deposition degree, which assesses the effect of pulsatile flow on deposition length. We performed several tests to determine how molecular weight affected these efficiency parameters. These tests examined (a) the effect of the injected cluster quantities, (b) the effect of the magnet distance, and (c) the effect of the injection period. Our findings indicate that an increase in PEG's molar weight significantly impacts magnetic particle targeting efficiency.

Keywords: magnetic targeting; nanocluster; polyethylene glycol (PEG); molecular weight; targeting efficiency; solvothermal method; deposition length; vessel obstruction

check for updates

Citation: Bernad, S.I.; Bunge, A.; Ioncica, M.C.; Turcu, R.; Dan, M.; Socoliuc, V.; Susan-Resiga, D.; Bernad, E.S. Impact of the Different Molecular Weights of Polyethylene Glycol (PEG) Coating Agents on the Magnetic Targeting Characteristics of Functionalized Magnetoresponsive Nanoclusters. *Magnetochemistry* **2024**, *10*, 51. https://doi.org/10.3390/magnetochemistry10070051

Academic Editor: Evgeny Katz

Received: 1 June 2024
Revised: 3 July 2024
Accepted: 18 July 2024
Published: 19 July 2024

Copyright: © 2024 by the authors. Licensee MDPI, Basel, Switzerland. This article is an open access article distributed under the terms and conditions of the Creative Commons Attribution (CC BY) license (https://creativecommons.org/licenses/by/4.0/).

1. Introduction

CVDs have ranked as the world's top cause of mortality for several decades [1]. Over half a billion people worldwide still suffer from cardiovascular problems. A considerable rise from the 12.1 million CVD deaths recorded in 1990, 20.5 million individuals died from cardiovascular disease in 2021, accounting for about one-third of all deaths worldwide [1]. These days, ischemic heart disease ranks as the leading cause of early mortality in 98 nations for women and 146 countries for men. The recorded statistics for 2021 demonstrate a notable rise from the data given in [2] for 2019, when the expected number of deaths from CVDs was 18.6 million (9.6 million men and 8.9 million women).

Drug therapy is the best and most effective way of treating CVD. Drug injection is a prevalent method in which only a small amount of the drug reaches the target spot, and the remainder is distributed throughout the body. For this reason, a large amount of medication must be injected to cure the disease, which has various side effects. The spread of drugs in the circulatory system reduces drug concentration in diseased tissue and has other side effects on human health [3].

The introduction of magnetic drug targeting (MDT) in the clinical treatment of CVD will enable drugs with short half-lives to obtain sufficient blood circulation time and, achieve drug accumulation at the target site. This will avoid dose-dependent side effects and decrease patient compliance due to repeated drug administration, achieving twice the impact with half the effort [4].

Encapsulating a drug increases the efficacy of various pharmaceutical compounds and reduces lateral effects. Furthermore, nano-based drug formulations can continue circulating for longer after injection by staying hidden from the body's defences, such as the mononuclear phagocytic system, thus increasing therapeutic effects [5]. One of the keys to treating CVD with the help of nanocarriers is passive accumulation, also known as passive or primary targeting, using the enhanced permeation and retention (EPR) effect [6]. The EPR effect can also be exploited to deliver biomaterial and passive–drug formulations to the inflamed site through the leaky vasculature surrounding inflamed tissue [6] (vascular inflammation is common in the pathogenesis of atherosclerosis). The extravasation of nanoparticles depends on various factors such as vascular wall permeability, the concentration of nanoparticles in the blood, and the nature of the vessel microenvironment in the diseased segment.

The intracellular magnetism of magnetic nanoparticles (MNPs) has been reported to disrupt the endothelial barrier at the target site and increase endothelial permeability, thereby enhancing site-specific drug delivery [7], making the application of MDT in CVD more promising.

Magnetite clusters are (normally spheric) particles of nano- or micro-size that consist of several to several hundred distinct magnetite nanoparticles bound together, more or less irreversibly, by aggregation, electrostatic interaction, and polymeric interlinkage [8].

Recent studies have shown that it is possible to synthesise iron oxide nanoparticles in non-spherical shapes, such as cubes [9], hexagons [10], and rods [11]. The nanoparticles' performance in biological applications mostly depends on their anisotropy and saturation magnetization [10,11]. For instance, elongated nanoparticles, nanodisc nanoparticles, nanocubes, and nanoflakes have been found to be more effective in magnetic hyperthermia than nanospheres [11]. It can be advantageous to use clusters instead of single particles of a similar size because they show no or less magnetic hysteresis than the respective single particles of a similar size while having similar or even increased [12] (due to particle–particle interactions) saturation magnetization compare to the nanoparticles they consist of, leading to potentially greater stability in suspension.

Many approaches have been investigated to tackle the challenge of NP instability in biological fluids [13,14]. First introduced in 1994 in a landmark paper by Gref and his colleagues [15], polymeric nanoparticles grafted with polyethylene glycol (PEG) can circulate in the blood for an extended period owing to the passivation effect of PEG.

The so-called "PEGylation" strategy is a common practice to guarantee efficient NP dispersion time. Using PEG to coat nanoparticles (NPs) has many advantages, such as reduced aggregation, phagocytosis, and opsonization, which decrease NPs immunogenicity and improve blood half-life; in other words, it enhances systemic circulation. PEG coating on NPs reduces their nonspecific adsorption of serum proteins and their uptake by the mononuclear phagocytic system [16]. Even if proteins can interact with the PEG coatings, the recognition systems fail to identify the underlying NPs as foreign bodies; in fact, PEG modification considerably increases NPs' circulation times.

Although the PEGylation of NPs provides a post-synthetic reproducible functionalization system for enhancing colloidal stability in physiological media, it causes an increase

in NP hydrodynamic size and, especially during in vivo experiments, the host can often develop antibodies against PEG-encapsulated nanocarriers [17]. After localizing at the target site, however, PEG coatings can substantially inhibit other functions, such as drug release and particle–cell interaction, potentially leading to diminished therapeutic outcomes compared to non-PEGylated carriers [18].

1.1. Some Aspects Regarding PEG

PEGs of different molecular weights and characteristics can be synthesised. Commercially available PEGs range in molecular weight from 200 to 35,000 Da and come in a variety of shapes and degrees of branching [19].

PEG is metabolised by the gradual oxidation of its hydroxyl group to generate carboxylic acid, diacids, and hydroxy acid metabolites after reaching systemic circulation; this is catalysed by the alcohol dehydrogenase enzyme [19] and certain other oxidase enzymes, such as cytochrome P-450. The renal route largely excretes PEG molecules (20,000 Da), whereas the biliary route mostly excretes PEGs with molecular weights ranging from 20,000 to 50,000 Da [19]. Liver macrophages typically absorb PEGs with molecular weights of more than 50,000 Da.

Poly(ethylene glycol), or poly(ethylene oxide), refers to an oligomer or polymer of ethylene oxide in linear or branched structures [20]. PEG is a hydrophilic polymer that can be adsorbed or covalently attached to the surface of nanoparticles.

PEG's chain length, shape, and density on the particle surface are the main parameters affecting nanoparticle surface hydrophilicity and phagocytosis.

Gref et al. [15] systematically studied the effect of PEG chain length in preventing protein adsorption on the surface of nanoparticles. The results showed that an optimal molecular weight (Mw) range exists (between 2 and 5 kDa) to reduce plasma protein adsorption. The amount of protein absorbed on poly(lactic co-glycolic acid) (PLGA) coated with polyethylene glycol (PEG—PLGA-PEG 5 kDa—was substantially reduced (∼80%) compared to the amount of non-PEGylated PLGA nanoparticles. Similarly, Fang et al. [21] have recently shown the effect of the molecular mass of PEG for passive targeting. The paper showed that the amount of protein adsorbed was directly dependent on the molecular mass of PEG. Medium-sized PEGylated nanoparticles (100–200 nm) showed 10–40% protein absorption, and PEG 10 kDa was found to be the most efficient size of PEG, compared to PEG 2 kDa and PEG 5 kDa for preventing protein absorption. The results suggest that dense PEG shielding over a negatively charged surface is essential in avoiding protein absorption.

PEGylation has steric-limiting effects on nanocarriers, making it more difficult for PEGylated treatments to interface with blood proteins and the mononucleated phagocyte system (MPS).

The PEGylation of proteins and other biomolecules can help reduce their immunogenicity and shield sensitive molecules from proteolytic enzymes, slowing down their breakdown [22]. Attracting water shells from associated PEG chains also helps PEGylated products become larger and prevents their rapid clearance by the kidneys. Therefore, PEGylated medicines demonstrate fewer side effects, improved pharmacokinetic characteristics, and excellent stability [23].

In addition to regular usage in cosmetics and many other home items, polyethylene glycol is a synthetic polymer extensively employed in the medical and pharmaceutical domains. Ensuring PEGylated treatments are safe and efficient in clinical environments depends on PEG immunogenicity, which is a significant challenge.

Much evidence has indicated that the administration of some PEGylated medications to individuals results in the production of anti-PEG antibodies, which are antibodies specifically targeted against PEG molecules [24]. Also, many investigations have shown that various PEGylated treatments cause anti-PEG antibodies that accelerate the blood clearance phenomenon (ABC), therefore impairing the pharmacokinetic behaviour of the second given dosage [25]. Although PEGylation is regarded as an excellent strategy to

lower immunogenicity, some investigations have revealed hypersensitivity responses (HSR) following the injection of various PEGylated medicines [26]. PEGylated treatments can stimulate the host immune system, leading to acute HSRs [27].

1.2. Problem Description

Two elements related to the control and capture of magnetic nanoparticles must be addressed for proper magnetic drug-targeting therapy. First, the particles must be guided across many artery bifurcations from their injection site before reaching the disease region. Second, after the particles enter the artery closest to the affected area, we must keep them there so the medications they contain may permeate the surrounding tissue. By conducting experimental studies on nanocluster depositions under various conditions, we attempt to address these issues.

First, we try to direct and trap the functionalized nanocluster in a straight tube under medium-sized artery-like flow conditions. Secondly, we try to guide a magnetic particle cluster under multiple settings, including the following:

(a) Varied injection durations.
(b) Variable mass concentrations of the injected MNCs.
(c) Different magnet distances from the desired location.

Below, we describethe specifics of the experimental inquiries and outcomes.

The primary objective of our research is to investigate the effects of three distinct PEG mass weights on the colloidal structure of suspensions of functionalized magnetic nanoparticles in a magnetic field. We aim to understand how these modifications influence the efficiency of cluster depositions during the targeting procedures in different operating environments. This knowledge could significantly enhance the effectiveness of magnetic drug-targeting therapy.

2. Materials and Methods

2.1. Nanocluster Synthesis and Characterization

Magnetite clusters can principally be synthesized in a one-step and a two-step procedures [28,29]. The two-step procedure consists of primarily synthesizing magnetite nanoparticles and, in the second step, clustering them together using a polymer. The main advantage of this method is that it provides excellent control over the size and properties of the single magnetite particles since the synthesis method can be freely chosen. The second step often uses surfactants or polymers in a mini-emulsion process [30].

Magnetite clusters can also be synthesized in a one-step process, and the main method used is a polyol reduction reaction. In the polyol method [31,32], typically performed under solvothermal conditions [33], iron salts are directly used as a precursor without synthesizing the nanoparticles first. Aside from the simplicity of the procedure, this method offers a wide variety of potential coatings [23,34] and, good crystallinity of the final clusters [35], as well as the possibility to tailor cluster and particle size, for example, by varying the solvent composition [36] or the basicity of the reaction mixture [37].

2.1.1. Synthesis

Ferric chloride hexahydrate ($FeCl_3$*H_2O), sodium acetate (anhydrous), polyethylene glycol (PEG-2000 and PEG-10,000), and ethylene glycol (99%) were purchased from Alfa Aesar (Kandel, Germany). Diethylene glycol (99%) was obtained from Sigma-Aldrich (Steinheim, Germany). Polyethylene glycol PEG 6000 was obtained from Thermo Scientific (Dreieich, Germany).

The synthesis of magnetite clusters via the solvothermal polyol reaction is shown in Figure 1. The synthesis was modified from [38], using polyethylene glycol (PEG) as the coating and adjusting the cluster size by the ratio of ethylene/diethylene glycol. Ferric chloride hexahydrate (4.34 g, 16.1 mmol), sodium acetate (10 g, 122 mmol), and PEG (PEG-2000, PEG-6000, or PEG-10,000, 4 g) were stirred with diethylene glycol (140 mL) and ethylene glycol (22 mL) for 1 h. The mixture was then transferred into a Teflon-

lined autoclave (200 mL) and heated at 200 °C for 15 h. The sample was washed with distilled water into a beaker, magnetically separated, and washed another four times. It was stored as a suspension in water. The samples were named MNC-2000, MNC-6000, and MNC-10,000, respectively.

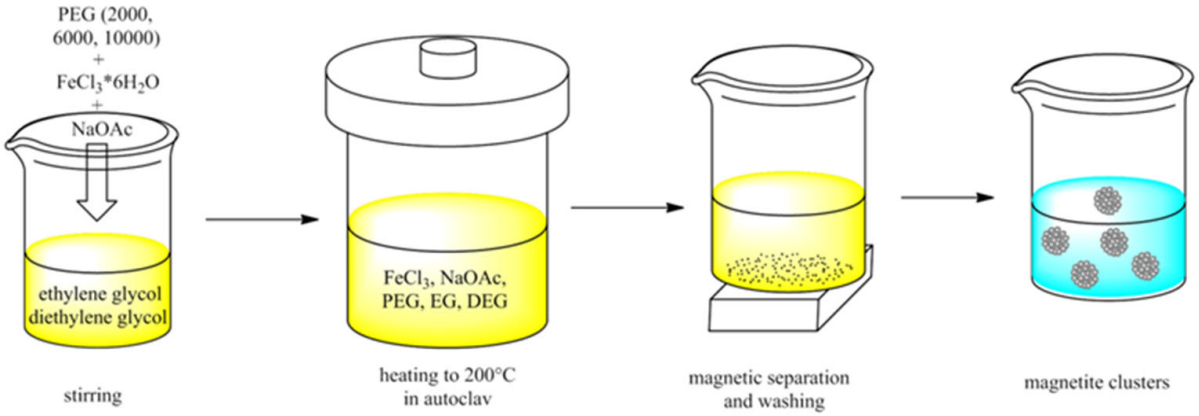


Figure 1. Schematic view of the reaction steps to obtain magnetite clusters dispersed in water.

2.1.2. Transmission Electron Microscopy (TEM) Investigation

The size and shape of the nanostructures were examined by scanning transmission electron microscopy (STEM) with a Hitachi HD2700 equipped with a cold field- emission gun and Dual EDX System (X-Max N100TLE Silicon Drift Detector (SDD) from Oxford Instruments, Oxford, UK). For the analysis, a suspension of the samples was sonicated (<10 s) with a UP100H ultrasound finger and deposited by the droplet method on a 400-mesh copper grid coated with a thin carbon layer. The nominal operating tension was 200 kV.

2.1.3. Thermogravimetry (TGA) Investigation

Thermogravimetry analysis (TGA) was performed with a Pyris 1 TGA (Perkin Elmer, Shelton, CT, USA) analyser in a temperature range from 30 to 1000 °C with a heating rate of 30 °C/min under air.

2.1.4. X-ray Photoelectron Spectroscopy (XPS)

A SPECS XPS spectrometer equipped with an Al/Mg dual-anode X-ray source, a PHOIBOS 150 2D CCD hemispherical energy analyser, and a multichanneltron detector with vacuum maintained at 1×10^{-9} Torr were used to record the XPS spectra. The Al K_α X-ray source (1486.6 eV) was operated at 200 W. The XPS survey spectra were recorded at 30 eV pass energy and 0.5 eV/step. The high-resolution spectra for the individual elements (Fe, C, O) were recorded by accumulating ten scans at 30 eV pass energy and 0.1 eV/step. Data analysis and curve fitting were performed using CasaXPS software version V10 with a Gaussian–Lorentzian product function and a nonlinear Shirley background subtraction. Peak shifts due to apparent charging were normalized with the C1s peak set to 284.8 eV. The high-resolution spectra were partly deconvoluted into the components to determine the bond types at the sample surface.

2.1.5. Fourier Transform Infrared (FTIR)

Fourier transform infrared (FTIR) spectra were recorded using a JASCO FTIR 4600A spectrophotometer with an ATR-PRO-ONE accessory, and were CO_2-, H_2O-, ATR−, and baseline-corrected as well as normalized for better visibility of the bands.

2.1.6. Dynamic Light Scattering (DLS) Measurements

A Malvern Zetasizer Nano-ZS device (Malvern Panalytical Ltd., Malvern, UK) outfitted with a He-Ne laser (λ = 633 nm, max 5 mW), operating at a scattering angle of 173°, was used to quantify the particles' hydrodynamic size and zeta potential. Before the measurements, the samples were diluted to a 0.1 mg/mL concentration. One millilitre of particle suspension was used in each measure.

2.1.7. Clusters' Magnetic Characterization

The magnetization curves of the PEG-coated clusters were measured using a vibrating sample magnetometer (VSM 880-ADE Technologies, Westwood, MA, USA) at room temperature in the field range of 0–1000 kA/m.

2.1.8. Rheology

The magneto-viscous characteristics of the PEGylated nanoparticles were tested at 25 °C in both the presence and absence of a magnetic field using a rotating rheometer (Anton Paar MCR 300 Physica, Anton Paar GmbH, Graz, Austria) with a 20 mm diameter plate–plate magnetorheological cell (MRD 170/1T-SN80730989, Graz, Austria). In this cell, a perpendicular magnetic field is applied to the sample layer situated between the plates. A Hall probe installed under the bottom plate of the MR cell measures the magnetic flux density of the applied magnetic field.

2.2. Magnetic Field Generation

The drag force of blood, which is higher in the centre of blood arteries than close to their walls, propels the movement of nanoparticles in the circulation. Magnetic fields can overcome this drag and facilitate the collection of magnetic nanocarriers. The magnetic field's intensity can enhance penetration by causing particles to gather on the vessel wall or to reroute close to the magnet [4,39]. These actions lessen adverse effects and cause a buildup of nanocarriers in the targeted tissue, enhancing the EPR effect and demonstrating significant promise in therapy for CVDs.

To approximate what might occur in vivo, we can examine MNC retention in vitro. Thus, it is possible to investigate the effects of many parameters on the effectiveness of magnetic targeting, including magnet design, flow speed, particle surface characteristics, distance from the magnetic pole, and particle size.

Drawing on previous research [40,41], this work aims to create a powerful magnetic field using a single external permanent magnet system, which will be utilized to draw, direct, and transport MNCs to the targeted area of the artery.

To produce the magnetic field in our experiment, we employed a rectangular NdFeB52 permanent magnet with, dimensions of 30 × 20 × 20 mm (length × width × thickness) (Figure 2A) and a maximum energy product (B × H) of 52 MGOe.

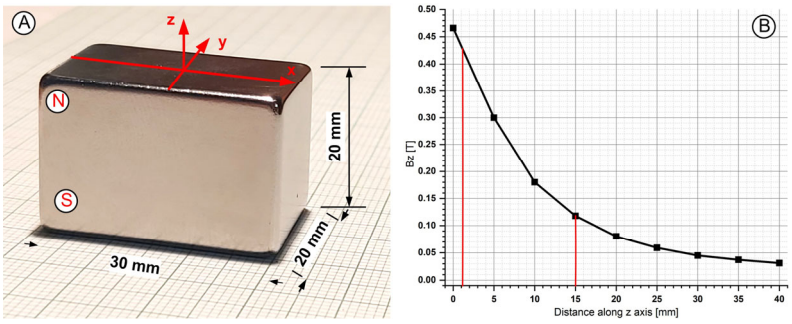


Figure 2. A magnetic field generated with the NbFeB52 permanent magnet was used in the experimental investigation. (**A**) The dimensions of the used magnet and axis association. The used permanent magnet had polarization along the Z-axis. (**B**) B_z evolution function of magnet surface distance.

The real B-field strength was determined at several positions along the magnet's central axis using a Tesla meter (Model 5080, F.W. Bell Gaussmeter, Milwaukie, OR, USA) positioned using a micrometre. In Figure 2B, the B-field magnitudes along the central axis of interest show an exponential decrease with distance, peaking at 430 mT at 2 mm and dropping to 0.03 mT at 4 cm from the magnet's base. In this experiment, the magnet produced a magnetic field strength of 0.43 to 0.12 T, which was positioned 2 to 15 mm from the vessel wall (Figure 2B). The intention was to observe the effects of the magnetic field on MNC targeting.

To capture particles, we provided a constant magnetic field to the target region. The magnetic field around the permanent magnet (Equation (1)) was calculated from [4,42], and it is defined as the density of magnetic lines of force, or magnetic flux lines, passing through a certain area.

$$\vec{B} = \mu\left(\vec{H} + \vec{M}\right), \tag{1}$$

where $\vec{B}$ (T) is—magnetic flux density, μ is the magnetic permeability of the medium, $\vec{H}$ (A/m) is the induced magnetic field, and $\vec{M}$ (A/m) is the magnetization of the material.

$$\mu = \mu_0 \mu_r, \tag{2}$$

where $\mu_0 = 4\pi \times 10^{-7}$ (H/m) is the magnetic permeability of free space, and μ_r is the relative magnetic permeability.

Magnetic flux density and magnetic field are related simply in free space, with magnetic flux density being proportional to magnetic field intensity (Equation (3)).

$$\vec{B} = \mu_0 \vec{H}, \tag{3}$$

A theoretical study for the magnetic field distribution around a rectangular permanent magnet can be found using Equation (5) ([43]):

$$B(z) = \frac{B_r}{\pi}\left(\tan^{-1}\frac{WL}{2z\sqrt{4z^2+W^2+L^2}}\tan^{-1}\frac{WL}{2(z+T)\sqrt{4(z+T)^2+W^2+L^2}}\right), \tag{4}$$

where W is—magnet width, L is—magnet length, T is—magnet thickness, B_r—is the magnet residual flux density, and z is the—distance from the magnet surface (where $z \geq 0$) to the magnet's centre line. In our case, W = 20 mm, L = 30 mm, and T = 20 mm (Figure 2A).

Based in our previous experience [40] the experimentally measured evolution of the Bz value is in good agreement with the evolution obtained using Equation (4).

2.3. Experimental Test Section

Our prior work [44] included a comprehensive description of the setup's general concept, and our earlier paper [45] explained the targeting mechanism in detail. To put it briefly, the experimental configuration replicates capturing MNCs from the flow and forming cluster deposits on the vessel wall. A variable-speed infusion pump (GAMPT mbH, Merseburg, Germany) was used to introduce 20 millilitres of the model suspension into the flow stream at 19d (d is the inner diameter of the glass tube) in front of the targeted portion. This was performed under pulsatile flow conditions. The magnetic capture of MNCs in the test section was seen using a CCD camera, which captured the magnet-induced MNC retention in the glass tube.

It is essential to mention that the working fluid is a blood-analogue fluid prepared by mixing calculated weights of distilled water and glycerol. It has a density (ρ) of 1055 kg/m^3—the same as blood. The model suspensions were prepared by mixing 20 millilitres of distilled water and 40 or 50 mg of the investigated MNCs.

The glass tubing had several benefits, even if the glass-like vascular tubes (Table 1 and Figure 3) did not reproduce natural blood vessels' biological and mechanical properties. These advantages include observing the hemodynamics more easily due to the vessel wall's high transparency and the ability to measure the length and location of the deposits in relation to the used magnet's centre.

Table 1. Geometric characteristics of the experimental test environment.

Total Length L [mm]	Inner Diameter d [mm]	External Diameter D [mm]	Glass Tube Thickness th [mm]
200	3	8	2.5

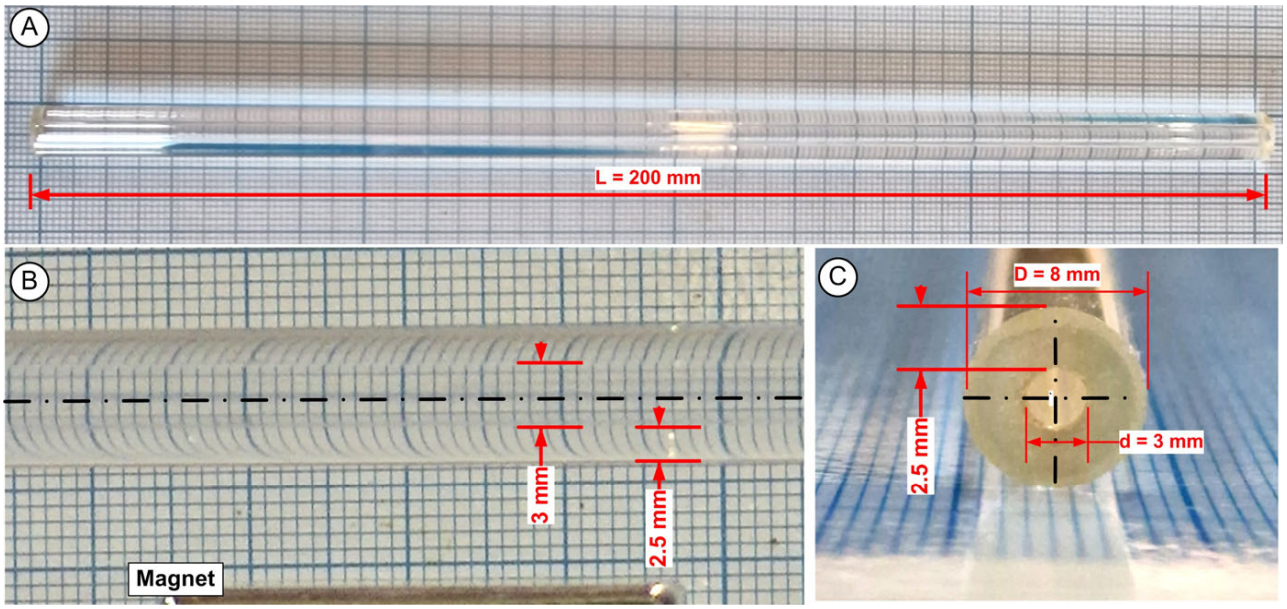


Figure 3. Experimental artery models. Glass tubing with a length of 200 mm, an inner diameter of 3 mm, and an external diameter of 8 mm makes up the test environment. (**A**) lateral view of the test section, (**B**) detail regarding the vessel internal diameter, (**C**) cross section of the used experimental vessel.

3. Results

3.1. PEG-MNC Size and Morphology

The magnetite clusters MNC-2000, MNC-6000, and MNC-10,000 were synthesized in a solvothermal polyol process. The polyol (in this case, ethylene glycol) serves as the reducing agent that partially reduces ferric to ferrous ions to form magnetite. The samples were easily suspendable in water because of the hydrophilic coating agents (PEG) used.

To determine the morphology of the three samples, TEM/SEM images were taken. Figure 4 shows TEM micrographs of the three types of nanoclusters. They have a well-defined shape, with a core–shell structure consisting of a cluster core with closely packed magnetite nanoparticles. For each sample, an image at higher magnification shows that an organic coating is also visible (Figures S1 and S2 in Supplementary File).

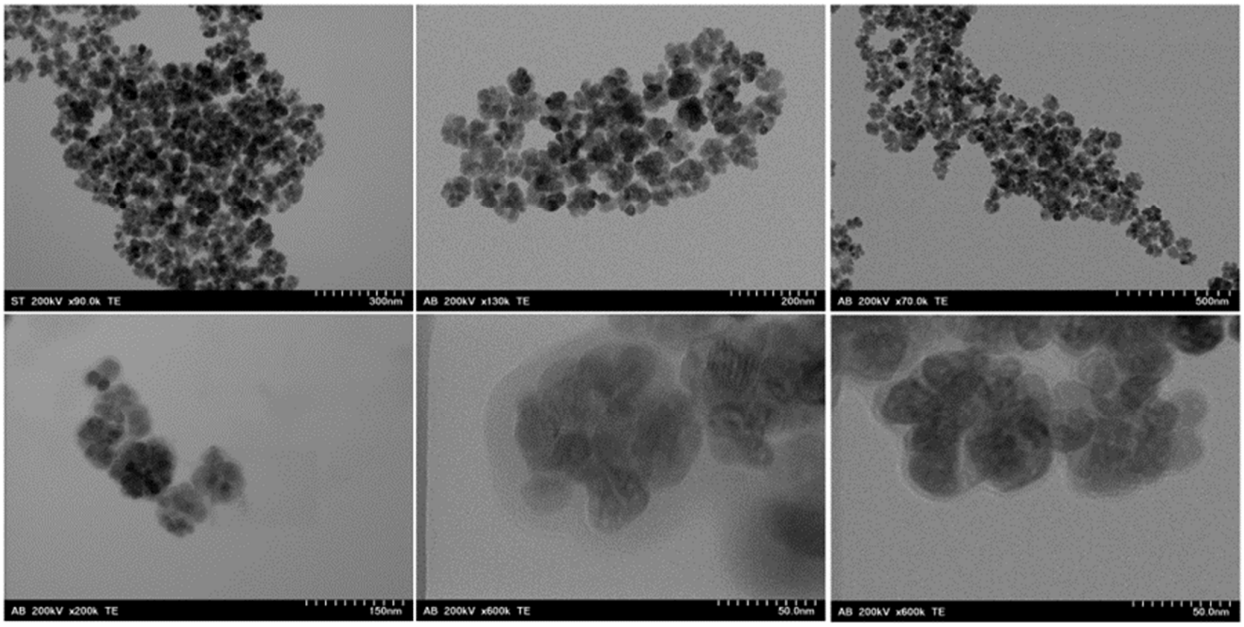


Figure 4. TEM images of MNC-2000 (**left**), MNC-6000 (**center**), and MNC-10,000 (**right**). On the bottom row, higher magnification images for the respective clusters show the coating layer distribution around the magnetite cluster.

In all cases, clusters were formed successfully. The clusters were relatively monodispersed, with sizes of 67 ± 11 nm for MNC-2000, 89 ± 9 nm for MNC-6000, and 80 ± 8 nm for MNC-10,000 (Figure 5).

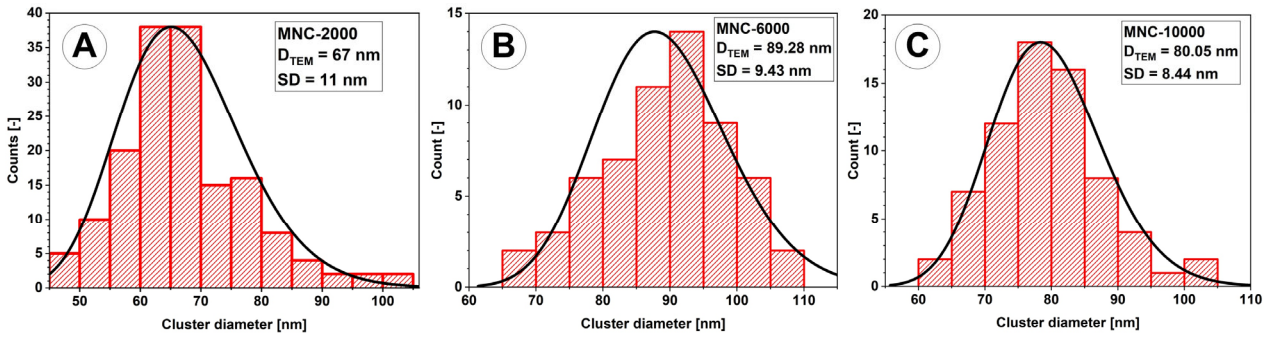


Figure 5. TEM size distribution and lognormal fit of the PEG-coated MNCs. The TEM size distribution was obtained by analysis of the TEM micrographs. (**A**) MNC-2000; (**B**) MNC-6000; (**C**) MNC-10,000.

Aside from a very small size change to smaller cluster sizes as the molecular weight of the coating agent increased, the samples were morphologically almost identical. In Figure 4 right, a cluster of MNC-10,000 is shown at a higher magnification, which allows the organic coating surrounding it to be seen.

The coating layer is uniformly distributed around the magnetite clusters. A similar coating layer was also observed in the other two samples (Figures 4 and S2 in the Supplementary Files). Due to the large particle size compared to the cluster size, the magnetite clusters are not perfectly round, but show a flower-like shape.

3.2. FTIR Investigation

The functional groups present in the magnetite clusters were analysed by FTIR (Figure 6). The spectra show typical signals of magnetite clusters synthesized by a solvothermal polyol process [38]. A band at 530 cm^{-1} stems from magnetite, whereas the broadband at 3000–3500 cm^{-1} is due to OH-stretching vibrations (ν(O-H)s). The absence of a band

at >650 cm^{-1} also confirms that magnetite, not maghemite, was formed [46]. The ν(O-H)s are both from the magnetite surface and the organic ligands forming the coating. In addition to PEG, ethylene glycol groups can also attach to surfaces [38].

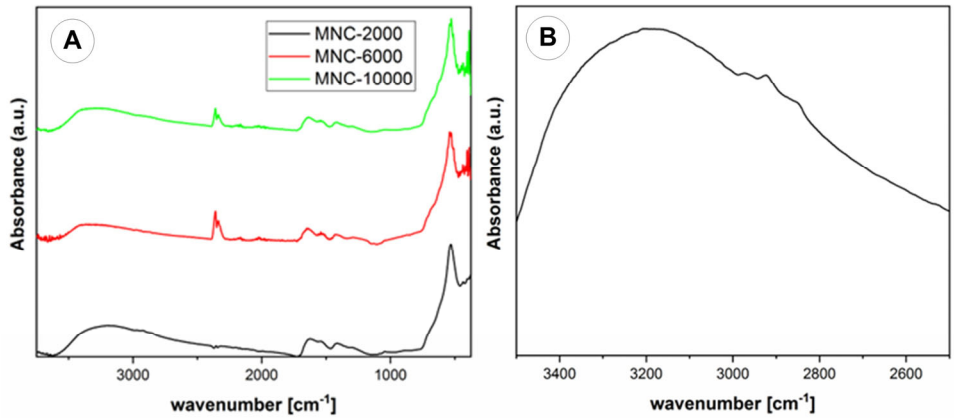


Figure 6. (**A**) FTIR spectra of samples of MNC-2000, MNC-6000, and MNC-10,000. (**B**) Zoomed-in view of the FTIR spectrum of sample MNC-2000.

The bands at 2843, 2908, and 2970 cm^{-1} are from ν(C-H) stretching vibrations (Figure 6B). All organic coatings, acetate, ethylene glycol, and PEG can contribute to these bands. In this case, the bands are relatively small. C-H stretching vibrations are generally not that intense compared to some other bands, but in this case, another reason could be that the amount of organic coating is comparatively low. At 1635 and 1417 cm^{-1}, the ν(C=O) bands of acetate attached to the magnetite clusters can be seen. A band at 1043 cm^{-1} (ν(C-O)) stems from ethylene glycol with PEG attached to the surface. Unfortunately, this band is very small in these samples, which makes it likely that the PEG coating layer is very thin again. This correlates with the TEM images, where the visible organic coating layer is relatively thin. The spectra of all three samples are very similar, which points to the fact that there are no notable differences in the functional groups or inorganic core for either sample.

3.3. TGA Investigation

To learn more about the coating thickness, TGA/DTA was performed on the samples (Figure 7). Interestingly, after a slight decrease until 120 °C, likely due to the desorption of physisorbed water from the surface, the mass increased in all samples to about 100.4% (100% for MNC-6000) of the original weight at 350 °C. While this is not a commonly observed phenomenon in the literature, it has been described before for magnetite nanoparticles [47].

This is not visible more often because, in many cases, TGA is performed in a nitrogen atmosphere, where such an oxidation event cannot happen. In other instances, mass losses from the desorption of tightly bound water or organic coatings can overlap with the mass gain from oxidation. This oxidation to maghemite is often observed up to ca. 200 °C, and the reason for it taking higher temperatures here might be because the particles that make up the MNC are comparatively large. At 590 °C for MNC-10,000,/593 °C for MNC-6000, 607 °C for MNC-2000, there are sharp decreases in mass. This is most likely from the organic coating. Interestingly, pure ethylene glycol, acetic acid, and polyethylene glycol [31] have much lower boiling points/show a mass decrease at a much lower temperatures in TGA.

The behaviour of the PEG-coated magnetite nanoparticles is similar [48]. This likely means that the MNCs' organic coating is much more tightly bound than usual and can likely only be released from the clusters by oxidation.

It is also interesting to note that mass loss happens at a slightly lower temperature in samples with higher-molecular-weight PEG. However, the total amounts of organics on the MNCs are relatively low, as the total mass loss of both samples at 1000 °C is only around 2.8%.

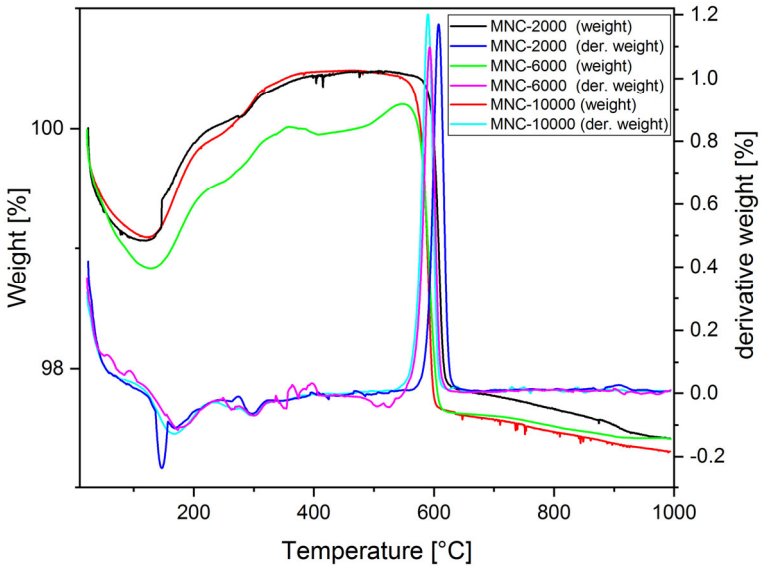


Figure 7. TGA and DTA curves of MNC-2000, MNC-6000, and MNC-10,000.

3.4. XPS Investigation

The chemical composition of the magnetic clusters covered with PEG polymers was analysed using X-ray photoelectron spectroscopy (XPS).

Figure 7 shows the high-resolution XPS spectra for the C1s, O1s, and Fe2p core levels of the magnetic clusters of the MNC-10,000 sample prepared using the solvothermal method. Similar spectra were obtained for the MNC-2000 and MNC-6000 samples.

The C1s spectrum in Figure 8 contains three components: the C-C (284.8 eV), C-O (287 eV), and O-C=O (289.5 eV) groups. The high intensity of the C-O component, both in the C1s spectrum and in the O1s spectrum indicates the presence of the PEG layer on the surface of the clusters. The Fe 2p spectrum contains the Fe 2p3/2 and Fe 2p1/2 doublet. The deconvolution of the Fe2p spectrum highlights the components corresponding to the iron oxidation state, with the octahedral Fe^{2+}, octahedral Fe^{3+}, and tetrahedral Fe^{3+} satellites being, characteristic of magnetite.

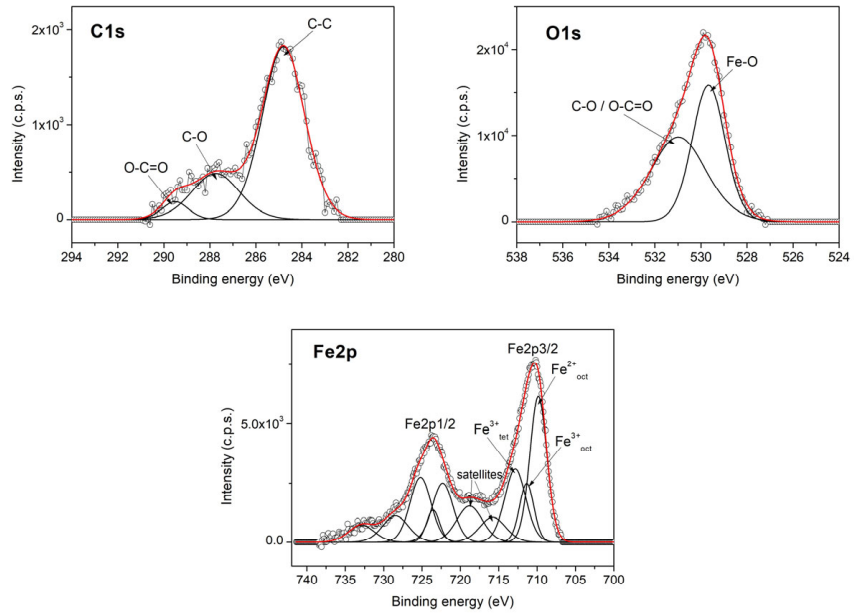


Figure 8. High-resolution XPS spectra of C1s, O1s, and Fe2p core levels with MNC-10,000.

The fitting parameters of the XPS spectra, including the peak positions (binding energy), full width at half maximum (FWHM), and calculated atomic concentrations from peak areas for the MNC-10,000 sample, are given in Table 2.

Table 2. Fitting parameters, including peaks positions, FWHM, and calculated atomic concentrations from peak areas for the MNC-10,000 sample.

Peak Name	Position (eV)	FWHM (eV)	% Atomic Concentration
C1s; C-C	284.8	2.1	11.3
C1s; C-O	287	2.4	3.6
C1s; O-C=O	289.5	1.3	0.7
O1s; Fe-O	529.6	1.7	27.5
O1s; C-O/O-C=O	531	2.8	29.3
Fe^{2+}_{oct} 2p3/2	709.84	2.6	4.7
Fe^{3+}_{oct} 2p3/2	711.36	2.2	1.7
Fe^{3+}_{tet} 2p3/2	712.85	3.2	2.9
Fe 2p3/2 satellite	715.8	4	1.3
Fe 2p3/2 satellite	718.8	4	1.8
Fe^{2+}_{oct} 2p1/2	722.32	3.2	4.5
Fe^{3+}_{oct} 2p1/2	723.56	2.02	1.6
Fe^{3+}_{tet} 2p1/2	725.2	3.2	5
Fe 2p1/2 satellite	728.47	4	2.5
Fe 2p1/2 satellite	732.8	4	1.6

3.5. DLS Investigation

We used DLS measurements to evaluate the stability of all three types of PEG-MNCs. We used a Malvern Zetasizer to assess the potential and zeta size of the examined suspensions.

Size distribution, zeta potential (ZP), and hydrodynamic diameter (zeta-average of the MNC) are three essential characteristics of the final PEGylated MNC that are revealed by dynamic light scattering (DLS). The electrostatic potential between an MNP's shear plane and the solvent is measured by the zeta descriptor, which also provides information on the stability of the MNP as a colloidal particle. The final product's homogeneity may be assessed using the size distribution parameter.

We applied PEG-2000, PEG-6000, and PEG-10,000 layers to the IONPs in our research. This process was crucial, as it gave the IONPs distinct surface charges and chemical properties, significantly influencing the PEG-MNC's behaviours in deionized water. The PEG-MNCs assumed a scattered colloidal form, as indicated by Table 3 and Figure 9.

Table 3. Zeta potential and size distribution by intensity of the PEG-MNCs in water.

Suspension	Average Hydrodynamic Diameter D_H [nm]	Zeta Potential [mV]	Polydispersity Index PDI
MNC-2000	628 ± 9	11.2 ± 0.4	0.548
MNC-6000	535 ± 16	13.1 ± 0.7	0.578
MNC-10,000	579 ± 8	4.82 ± 0.2	0.361

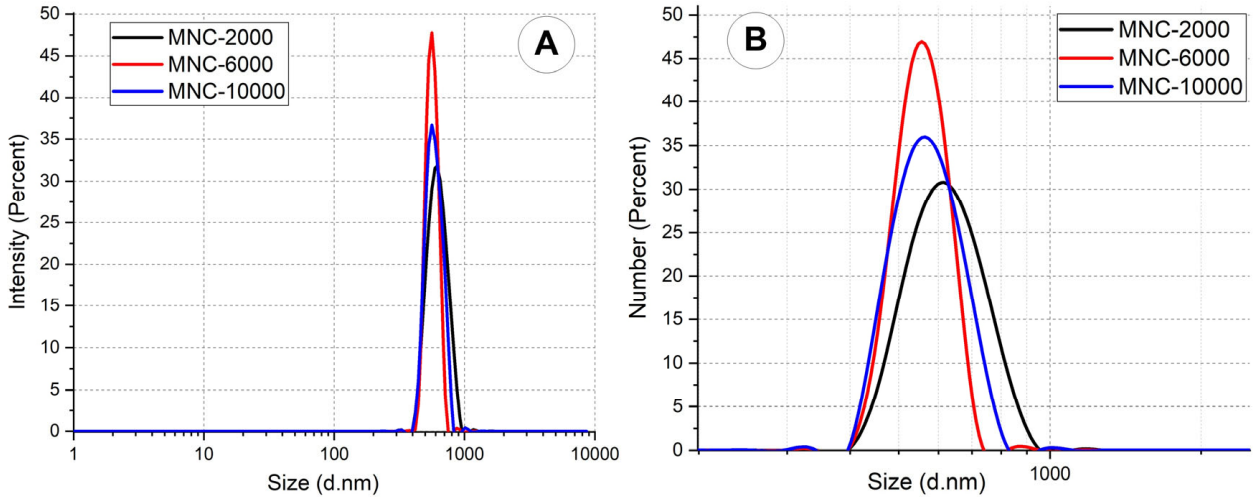


Figure 9. (**A**) Size distribution by intensity, and (**B**) number distribution for the PEG-MNCs' aqueous dispersions based on DLS investigations.

These suspensions had surface charges of 11.2 mV, 13.1 mV, and 4.82 mV, and average hydrodynamic diameters of 628 nm, 535 nm, and 579 nm for MNC-2000, NC-6000, and MNC-1000. The polydispersity index (PDI) was used to investigate the sample's aggregation, and the results were 0.548, 0578, and 0.361 for MNC-2000, MNC-6000, and MNC-10,000.

Based on the ZP magnitude, colloidal stability can be anticipated. With scores under −25 or higher than +25 mV, the ZP of NPs exhibits a high degree of stability by nature. Having a high ZP indicates highly charged particles that prevent electric repulsion and, hence, prevent particle aggregation. Van der Waals interparticle attraction causes attraction to overcome repulsion in low-ZP situations, which increases the likelihood of agglomeration, coagulation, or flocculation [49].

As shown in Figure 9, all the investigated PEG-MNCs with aqueous dispersion showed both polydispersity and a monomodal distribution, indicating the presence of large agglomerates. The ζ potential indicates repulsion between particles in a suspension. The low potential may explain the increased size, as increasing the attractive interactions between clusterspromotes particle aggregation [50]. However, MNC-10,000's measured ζ potential of 4.82 ± 0.2 mV is insufficient to prevent aggregation.

Several elements affect the functioning of a polymer; among them, Mw is very important in the formation of coatings on IONPs. Together with its concentration, the Mw of the polymer clearly affects the ultimate physicochemical characteristics of the coated nanoparticles. Within a suspension, ζ potential can indicate the degree of repulsion among particles [50]. Though PEG is a neutral-charge polymer, terminal hydroxyl groups give a little negative charge. The principal mechanism of PEG coatings on MNCs is surface adsorption, namely by the covalent bonding of the partly negative ether chain and the coordination bonding of the terminal hydroxyl group, according to all investigated MNCs showing a notable reduction in ζ potential. At last, the monodispersity (PDI of 0.361–0.578, Table 3) of the investigated MNCs in water stayed the same when PEGs with varying Mws were introduced, thereby indicating that this had no influence on their mean PDI. We must highlight the correlation between our results and Wilfred's findings in [50].

It is well accepted that positively charged nanoparticles have a higher cell uptake rate than neutral or negatively charged formulations. Nanoparticles carrying a positively charged surface are also expected to have a high nonspecific internalization rate and short blood circulation half-life. Nano shells with a negative surface charge have shown a marked reduction in uptake rate [51].

3.6. Rheological Properties of the Investigated Clusters

The rheological measurements for this article were meticulously carried out using an MCR 300 rheometer (Anton Paar, Stuttgart, Germany). In all rheological measurements, the MCN mass concentration was 0.5%. We applied a precise perpendicular magnetic field to the sample layer between the plates using a magnetorheological cell (plate–plate geometry) with a diameter of 2R = 20 mm and a gap set at h = 0.2 mm.

With a systematic approach, at a temperature of 25 °C, we measured the viscosity curves at various values (B = 0, 42, and 183 mT) of the magnetic flux density of the applied magnetic field with a range of shear speeds.

The suspension displays shear-thinning behaviour both in the magnetic field's absence (Figure 10A) and presence (Figure 10B). The applied magnetic field strongly influences all three magnetic nanofluids' flow behaviour (Figure 10B). Figure 10B shows that increasing the amplitude of the applied magnetic field leads to immediate cluster formation, increasing nanofluid viscosity. It is worth noting that the rise in viscosity happens only in the low-shear-rate zone, but shear thinning occurs at all other shear rates. The applied magnetic field produces strong interactions between magnetic nanoclusters, resulting in the development of magnetic structures. However, when the shearing rate increases, the structures of agglomerates degrade, and the nanoparticles organize themselves in the shearing direction. At high shear rates, fluid viscosity decreases.

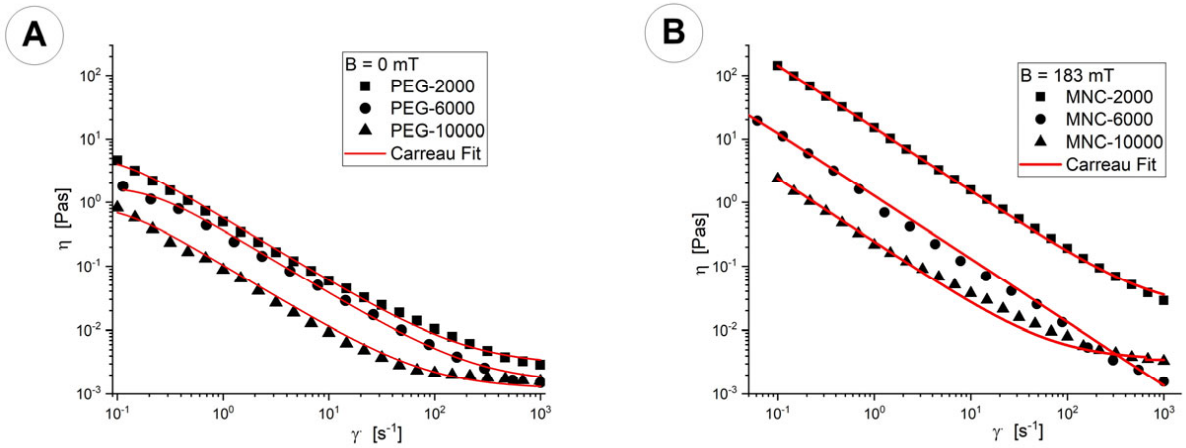


Figure 10. Rheological properties of the MNCs' aqueous suspension at the temperature of 25 °C. Viscosity curve in the absence (**A**) and presence (**B**) of the magnetic field. In all rheological measurements, the MCN mass concentration was 0.5%.

The obtained data were correlated with the Carreau model [52]:

$$\eta(\dot{\gamma}) = \eta_{\infty} + (\eta_o - \eta_{\infty})\left[1 + \left(C\dot{\gamma}\right)^2\right]^{-p}, \quad (5)$$

where C represents the Carreau constant at high values of the shear rate $\dot{\gamma}$, p [-] is the Carreau exponent, η_o is the viscosity at infinitely low shear rates, and η_{∞} [Pas] is the viscosity at infinitely high shear rates.

Figure 11A shows the impact of shear rate on the MV effect at B = 183 mT and the magnetic flux density levels at T = 25 °C. We find that the MV impact is nearly independent of shear rate at low shear rates, but becomes considerably smaller at high shear rates because of cluster agglomeration disintegration. The same conclusion can be drawn for the MV effect at B = 42 mT magnetic flux density levels (Figure S3A in the Supplementary Files).

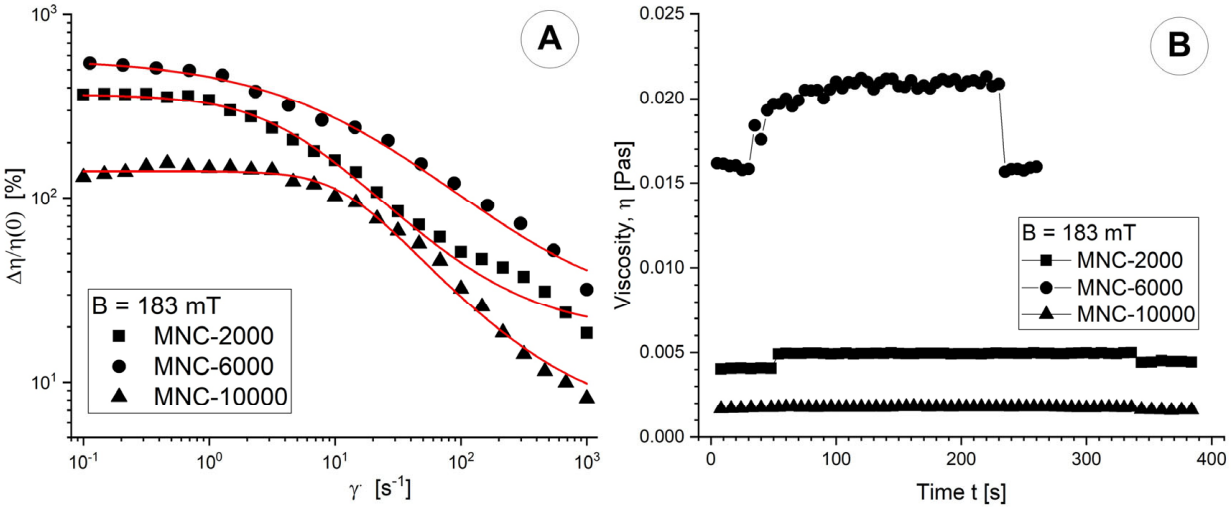


Figure 11. (**A**) Magneto-viscous effects (MVE) as a function of shear rate for magnetic flux densities of 183 mT; (**B**) Viscosity curve function of time for magnetic flux densities of 183 mT. In all rheological measurements, the MCN mass concentration was 0.5%.

The objective of the viscosity–time–magnetic field test was to ascertain the viscosity's time-dependent behaviour and the rate at which cluster agglomerations develop or disintegrate when an external magnetic field is applied or removed.

In our test, we avoided overly disrupting the development of particle agglomerations. We conducted the test with three intervals of constant low shear rate. The torque, a crucial factor, exhibited sufficiently high values (>5 μNm) to ensure the consistency of the experimental findings. We set B to 0 (each with six experimental points) for the first and last intervals, and for the second interval, we fixed B at 42 (183 mT). The temperature was set at T = 25 °C. The agglomeration phenomena achieve saturation 40 s after applying a magnetic field at a field strength of 183 mT (Figure 11B). In the absence of a magnetic field, slow agglomeration continues. Particle agglomerations can develop or break down extremely fast. Almost all the tested magnetic field strengths show that the suspension viscosity recovers to its pre-application value when the magnetic field is removed. At an applied magnetic field intensity of 42 mT, agglomerations are observed in the MNC-2000 and MNC-10,000 samples but not in the MC-6000 sample (Figure S3B in the Supplementary File).

3.7. Clusters' Magnetic Properties

In the current study, magnetic nanoparticle clusters, representing individual nanoparticles' magnetic moments, were created in a polymer shell using the solvothermal method. When a dry MNC sample is examined using a vibrating sample magnetometer (VSM), no hysteresis is visible in the magnetization curves (Figure 12).

These clusters are superparamagnetic at ambient temperature because remanent magnetization is not present. This matches our expectations, since the primary size of the investigated nanomagnets (D_{TEM} = 16.7 nm, 17.83 nm, and 12.87 nm for MNC-2000, MNC-6000, and MNC-10,000) is smaller than the superparamagnetic limit of the magnetite nanoparticles (>20 nm) [53]. The saturation magnetizations for PEG-coated MNCs are 80, 78, and 82 emu/g for MNC-2000, MNC-6000, and MNC-10,000 (Figure 12).

All samples have high saturation magnetizations M_s, with M_s being the highest for clusters coated with PEG-10,000, and slightly smaller ones for clusters coated with PEG-2000 and PEG-6000, in this order. The high magnetization compared to the bulk magnetization of magnetite (92 emu/g) [54] is another indicator that the organic coating is comparatively low, which agrees with the results obtained by the TGA. There are no significant differences in M_s between the three samples.

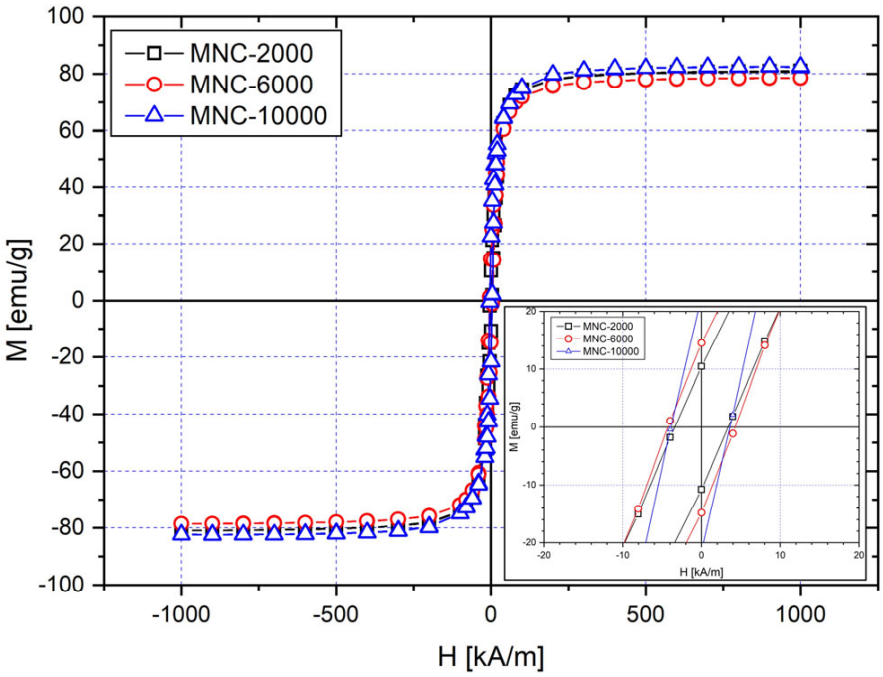


Figure 12. Magnetization curves for a sample of dry MNCs at room temperature (25 °C).

3.8. Clusters Deposition Analysis

Medicine delivery needs contact with the arterial wall when employing magnetic drug targeting (MDT). Magnetic nanoparticles (MNPs) only draw out the blood flow when they come into contact with the wall and then remain there. In this scenario, a powerful magnetic force component must hold a particle in position to oppose the drag force.

Using image analysis, we show the distribution of MNCs and analyse the depositions within the targeted region of the investigated artery segment. We used a Sony XC CCD camera to visualize and record the collection of MNCs on the tube surface.

We used ImageJ software, V4.2 or all our measurements regarding particle deposition characteristics (in terms of length, thickness, and the MNC deposition position regarding the magnet centre) (https://imagej.nih.gov/ij/, version 4.2, accessed on 2 May 2024).

Viscous and magnetic forces significantly influence the shape and quantity of MNCs deposited in the desired area. The shape of the accumulating particles also reveals the correlation of these forces during the injection phase.

In these studies, we performed the experimental measurements three times in the same manner for each investigated situation to demonstrate the effectiveness and consistency of the magnetic targeting procedure.

We set the deposition total length (L_t), the deposition thickness (Tn), the deposition proximal length (L_p), the deposition distal length (L_d), and the magnet distance from the artery wall (Dt) to see how different working conditions affect particle deposition (Figure 13). The magnet's size and the magnetic force's axial component were found to influence the length of particle deposition [40]. The vertical component of the magnetic force and the type of magnet used were primarily responsible for the thickness of the deposit [29].

Defined parameters for deposition, are crucial in biomedical applications, with practical implications. They help determine the appropriate medication dosage during treatment and aid in choosing the area of applicability (e.g., by determining the diameter of the targeted artery to avoid artery blockage or flow reduction induced by particle accumulation in the targeted site) for a specific magnet type. As mentioned previously, these defined deposition parameters are directly linked to the flow's hemodynamic force and the magnetic field's strength generated by the type of magnet used.

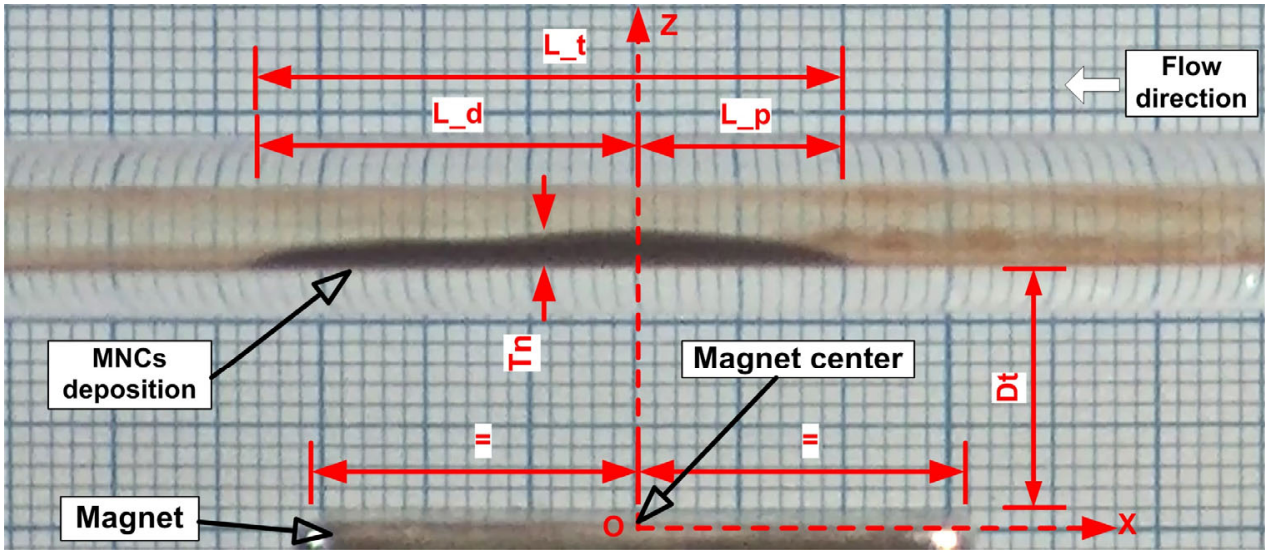


Figure 13. Geometrical characteristics of MNC deposition. L_t = deposition total length; L_p = proximal length; L_d = distal length; Tn = deposition thickness; Dt = magnet distance from the artery wall. L_p and L_d are measured from the magnet centre.

In the experiments, a pulsatile flow was applied at the artery model's inlet section (Figure 14, red line). This velocity function was calculated using an approximation of the coronary blood flow velocity reported in Liebergen's work [55]. Both velocity signals show significant acceleration and deceleration cycles corresponding to the heart cycle's systolic and diastolic phases.

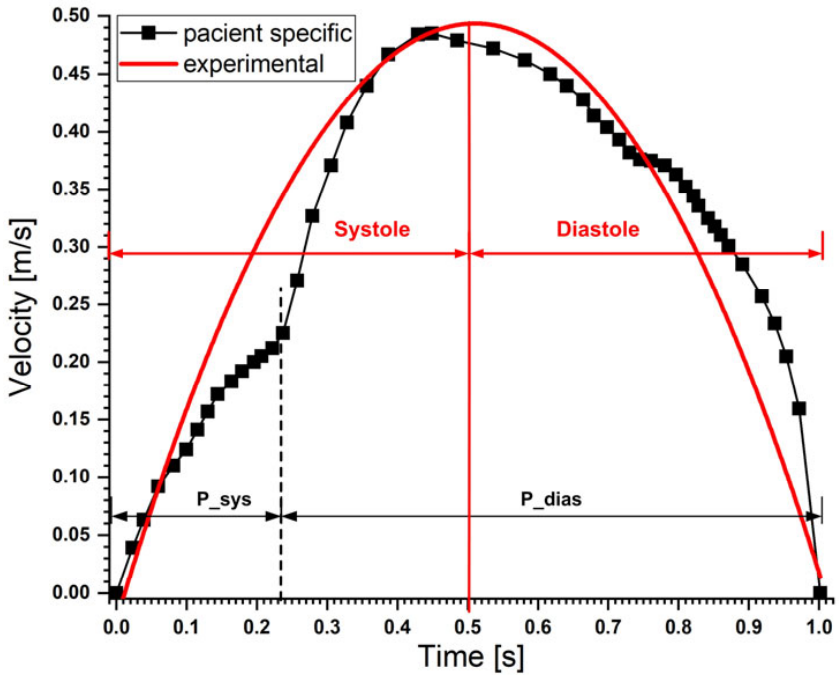


Figure 14. Pulsatile velocity signal used during targeted investigations.

We injected the suspension of magnetic clusters into the artery before the model artery inlet section, creating a three-dimensional magnetic material region. As a result, the generated magnetic force in the targeted region could slow and induce more successful MNC capture.

The fundamental function of magnetic drug delivery is to guide medicine to the illness location. When the magnetic nanocarriers reach their intended vessel segment, they accumulate along the vessel wall in a layer. In some conditions, the layer thickness can be enough to restrict the flow. This might cause high blood pressure and tissue hypoxia. Flow obstruction can occur due to a variety of factors, including the sort of magnet, distance to the targeted vessel (resulting in a large magnetic field that induces enhanced deposition), small vessel diameter (capillary), the large size of the nanomagnetic particles, or magnetic particle aggregation or agglomeration during targeting processes near the treated site.

To further comprehend and quantify the efficiency of each examined MNC in terms of magnetic drug targeting, we defined the following efficiency parameters:

(i) Obstruction degree (Equation (6)): Quantify the vessel obstruction grade following particle deposition.

$$OD = \frac{Tn}{d} \times 100, \quad (6)$$

where OD [%] is the obstruction degree, Tn [mm] is the deposition thickness, and d [mm] is the vessel's inner diameter.

(ii) The magnet coverage degree (Equation (7)) measures the quality of particle deposition along the vessel wall by measuring the deposition length considering magnet length.

$$MCd = \frac{L_t}{M_l} \times 100, \quad (7)$$

where MCd [%] is the magnet coverage degree, L_t [mm] is the deposition total length [mm], and M_l [mm] is the magnet length [mm] (in our case, 30 mm) (Figure 2).

(iii) The proximal deposition degree (Equation (8)) quantifies the pulsatile flow's impact on the deposition's shape and length.

$$PDd = \frac{L_p}{L_t} \times 100, \quad (8)$$

where PDd [%] is the proximal deposition degree, L_t [mm] is the deposition total length [mm], and L_p [mm] is the deposition proximal length [mm].

4. Discussion

Several factors influence how medications travel through the bloodstream: (i) the force of the injection (from the piston pump or syringe), (ii) the velocity profiles in the blood vessels, (iii) mixing due to red blood cells rotating and colliding, (iv) eddies at points where two streams meet, (v) changes in flows with heartbeat, and (vi) changes in flows in specific locations. In diseased arteries, velocity profiles and flow changes with the cardiac cycle are relevant, but regional flow variation is the most important factor.

The effectiveness of nanoparticle arterial localization is crucial for optimizing medication effects at the target location. As a result, we investigated numerous aspects that affect the successful deposition of nanoparticles in the targeted artery. In the following paragraphs, we look at the consequences of injecting different quantities of functionalized magnetoresponsive clusters, moving the magnet farther away, and varying the injection duration. All these characteristics impact the clusters' deposition effectiveness when coated with various molecular weights of PEG agent.

In our present study, we evaluated the magnetic accumulation of three types of MNCs with different molecular weights of coating agent: MNC-2000, which has a hydrodynamic diameter of 628 nm and potential of 11.2 mV; MNC-6000, which has a hydrodynamic diameter of 535 nm and a potential of 13.1 mV; and MNC-10,000, which has a hydrodynamic diameter of 579 nm and a potential of 4.82 mV (see Table 2). The chosen amounts of circulating clusters (40 or 50 mg, equivalent to 4 mg/mL or 5 mg/mL) were significantly lower than the maximum human-safe dose of the cancer drug doxorubicin used in breast

cancer treatment. "Doxorubicin can be given as an intravenous bolus (5 min), a short infusion (15–20 min), or as a 1- to 3-h infusion at doses ranging from 40 to 75 mg/m^2" [56].

4.1. Guiding, Capturing and Depositing the Clusters in the Targeted Area

When the magnetic field's force on the particles exceeds their hydrodynamic force, larger vessels (in our example, 3 mm in diameter) show magnetic capture under flow circumstances. The properties of the nanoparticles, gradients in the magnetic field, and flow dynamics may, therefore, significantly affect the behaviour of the magnetic particles in circulation.

Figure 14 shows how, when the permanent magnet remains in an exact location (5 mm from the artery's bottom wall), the quantity of MNC-6000 that accumulates in the artery varies over time. As seen at the end of the injection period, MNCs covered almost the whole magnet's pole face in the investigated geometry. Table 4 shows the evolution of particle deposition morphology in terms of thickness and deposition length over the injection period.

Table 4. Characteristics of the MNC-6000 deposition shape during the injection time of 60 s.

No	Injection Time [s]	Deposition Proximal Length L_p [mm]	Deposition Distal Length L_d [mm]	Deposition Total Length L_t [mm]	Deposition Thickness Tn [mm]	Magnet Distance Dt [mm]
1	0	0	0	0	0	11
2	3	7	14	21	0.2	
3	10	20	22	42	0.8	
4	20	18	20	38	1.1	
5	40	16	18	34	1.4	
6	60	14	17	31	1.5	

The magnetic field enhanced the interaction between the injected MNCs and fluid flow. Consequently, certain injected particles are carried downstream in the host vessel, while others are entrapped in the designated regions.

Our experimental studies found three different kinds of behaviour that were, very similar to those described in [57]:

(i) The produced magnetic forces in the velocity-dominated scenario could not capture the particles since they were weaker than the blood flow forces. As such, the nanoclusters came out of the blood vessels. This situation is presented in Figure 15A,B.

(ii) In the magnetic-dominated situation the magnet pulled the particles towards the vessel wall, and the magnetic forces much surpassed the flow force (Figure 15C).

(iii) Nanoclusters built up in a layer near the vessel wall in the boundary layer situation. When blood drag forces and magnetic forces were similar, the boundary layer regime was dominant (Figure 15D–F). Here, when the blood velocity was almost nil, the nanoclusters accumulated on the vessel wall.

In the cases shown in (ii) and (iii), it is critical to recognize the importance of the pulsatile flow regime in the nanocluster deposition process, notably in defining the length and ultimate shape of the deposition (see Supplementary Video S1).

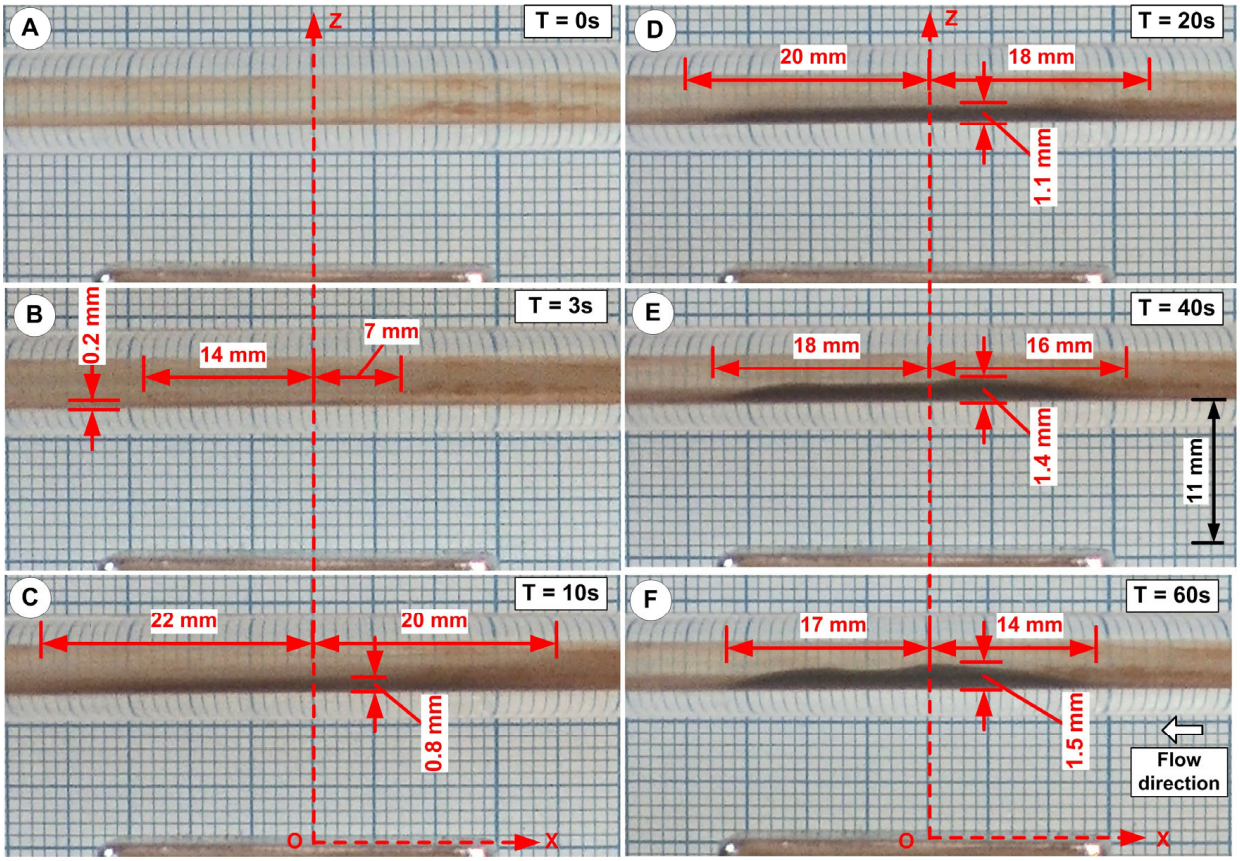


Figure 15. Cluster deposition during the injection period. Injection period of 60 s; injected cluster: MNC-6000. Snapshot of the deposition shape and length at six different time steps. (**A**) T = 0 s, (**B**) T = 3 s, (**C**) T = 10 s, (**D**) T = 20 s, (**E**) T = 40 s, and (**F**) T = 60 s (end of the injection period).

4.2. Influence of the Injected Quantity of the Functionalized Nanoclusters

The vessel and the magnet's axis are always orthogonal for all tested geometries, and clusters accumulate in low-lying "dunes" throughout the magnet's entire pole face.

The quantitative correlations between the distance from the artery's lower wall, cluster deposition positions and shapes of the investigated clusters with different Mws are presented in Table 5 and Figure 16. The measurements for all types of clusters were performed in identical working conditions, namely the pulsatile nature of the working fluid (Figure 14), an injection period of 60 s, and a magnet distance of 11 mm.

Figure 16 depicts the attraction of MNCs to the vessel's lower wall, which results in an unequal distribution along the magnet's horizontal axis. Furthermore, particle buildup changes the flow structure, affecting the cluster deposition's form.

Moreover, the induced deposition is divided into two distinct regions: a thinner region where the fluid flow washes away some of the collected MNCs (associated with the proximal deposition length L_p), and a thicker region where the magnetic field generated together with the effects of the pulsatile flow drives the capture of nanoclusters (associated with the distal deposition length L_d).

The morphology of the accumulating nanoclusters indicates the relationship between the magnetic and hydrodynamic forces throughout the particle-injection phase.

From our perspective, it is critical to note that the stated efficiency metrics (Equations (2)–(4)) refer to the fact that the collected clusters have a uniform distribution along the vessel wall to optimize drug transport and concentration in the targeted arterial segment. Medical professionals must interpret this efficacy to design a strategy that produces optimal deposition for desired treatments.

Table 5. Characteristics of the particle accumulation shape along the artery lower wall at the end of the injection period of 60 s for injected quantities of 40 mg and 50 mg for different types of magnetic clusters.

MNC Type	Injected Quantity [mg]	Deposition Proximal Length L_p [mm]	Deposition Distal Length L_d [mm]	Deposition Total Length L_t [mm]	Deposition Thickness Tn [mm]	Obstruction Degree [%]	Magnet Coverage Degree [%]	Proximal Deposition Degree [%]
MNC-2000	40	9	16	25	0.5	16.7	83.3	36
	50	10	21	31	0.5	16.7	103.3 *	32.3
MNC-6000	40	11	17.2	28.2	1.5	50	94	39
	50	5	30	35	0.5	16.7	116.6 *	14.3
MNC-10,000	40	10	18	28	1.3	43.3	93.3	35.7
	50	10	17	27	0.7	23.3	90	37

Note: * This indicates that the deposition length surpasses the length of the magnet. For example, in the case of MNC-2000, for injected quantities of 50 mg, the magnet coverage degree is 103.3%, which means that the deposition length exceeds the magnet length by 3.3% (103.3–100%).

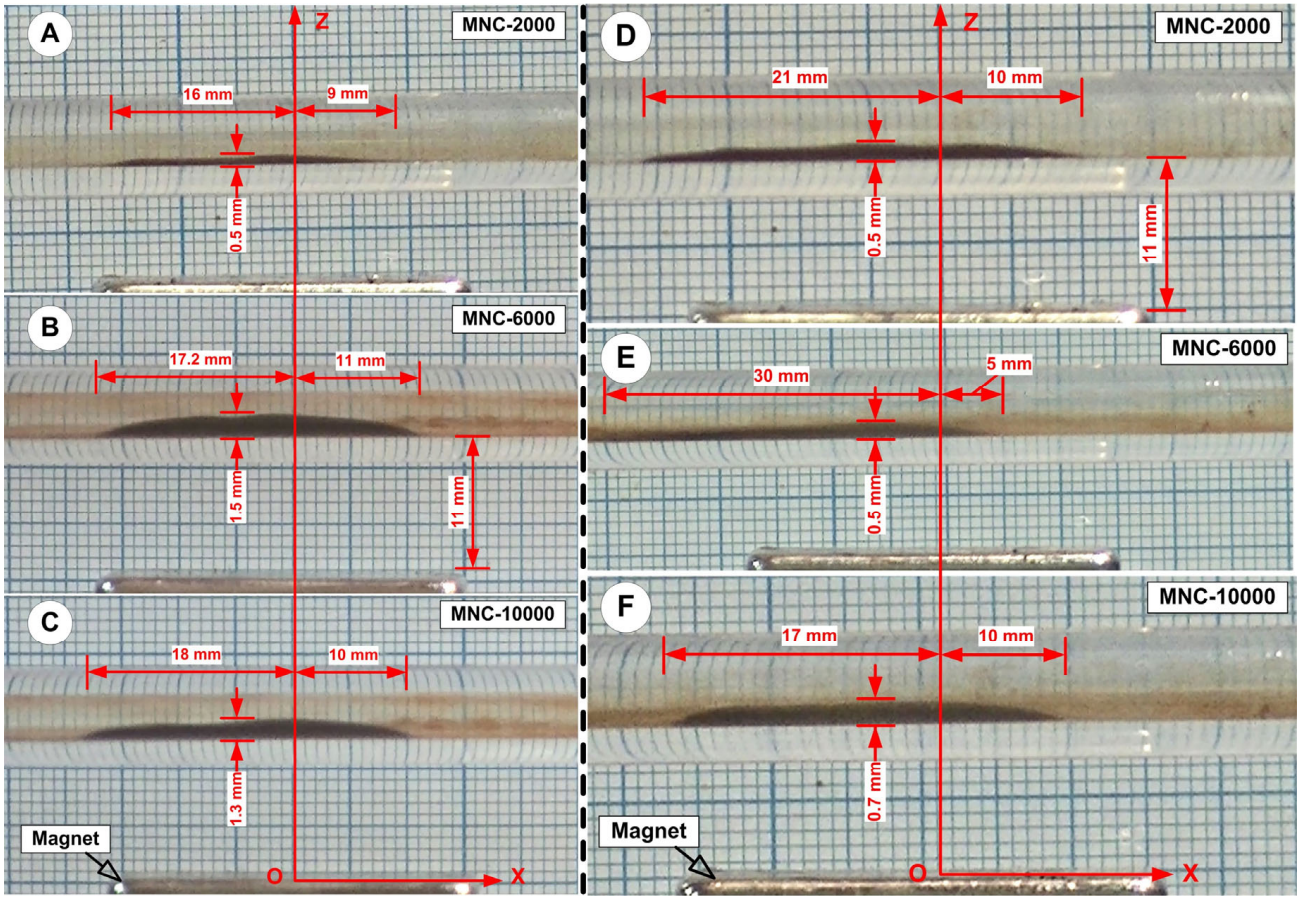


Figure 16. Figure shows the influence of the injected quantities on the deposition distribution on the vessel wall in the targeted region for the MNCs coated with PEG with different Mws. Injected quantity of 40 mg functionalized nanoclusters: (**A**–**C**). Injected quantity of 50 mg functionalized nanoclusters: (**D**–**F**). The injection time is 60 s for all experiments. Magnet distance from the vessel's bottom wall is 11 mm.

Figure 17 presents a comparative analysis of the different amounts of injected clusters for all investigated functionalization agent variants from the point of view of the defined efficiency parameters.

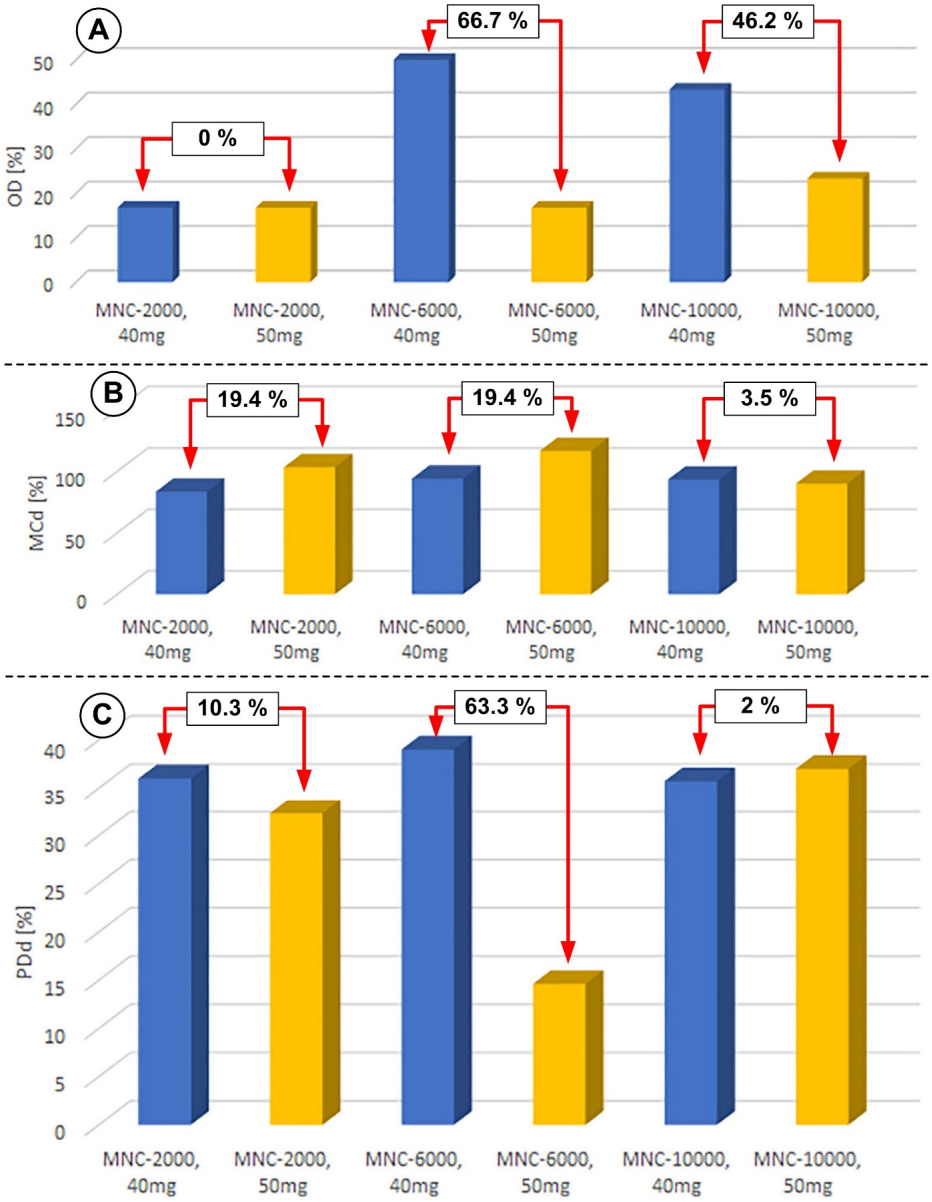


Figure 17. The impact of the injected cluster quantities on the defined efficiency parameters. (**A**) OD—obstruction degree; (**B**) MCd—magnet coverage degree; and (**C**) PDp—proximal deposition degree. All measurements were performed in the same conditions: pulsatile flow, injection period of T = 60 s, and the same magnet (NbFeB52) (magnet dimensions: 30 × 20 × 20; length × width × thickness).

The analysis of the degree of occlusion of the flow section reveals that the injection of 50 mg of clusters ensures a low degree of occlusion for all types of MNCs investigated (16.7% in the case of MNC-2000 and MNC-6000, and 23.3% in the case of MNC-10,000). Instead, the injection of 40 mg of clusters induces significant variations in the degree of obturation: 50% in the case of MNC-6000 and 43.3% in the case of MNC-10,000, compared to the degree of obturation of only 16.7% in the case of MNC-2000 (Figure 18A). From the point of view of magnet coverage, each injected cluster's quantities cover around 90% of the magnet length for all types of clusters investigated (Figure 18B). The same coverage tendency is also identified for the proximal part of the magnet for all kinds of clusters used,

except the MNC-6000 cluster, for which the injection of 50 mg induced a low degree of coverage in the proximal area of the magnet.

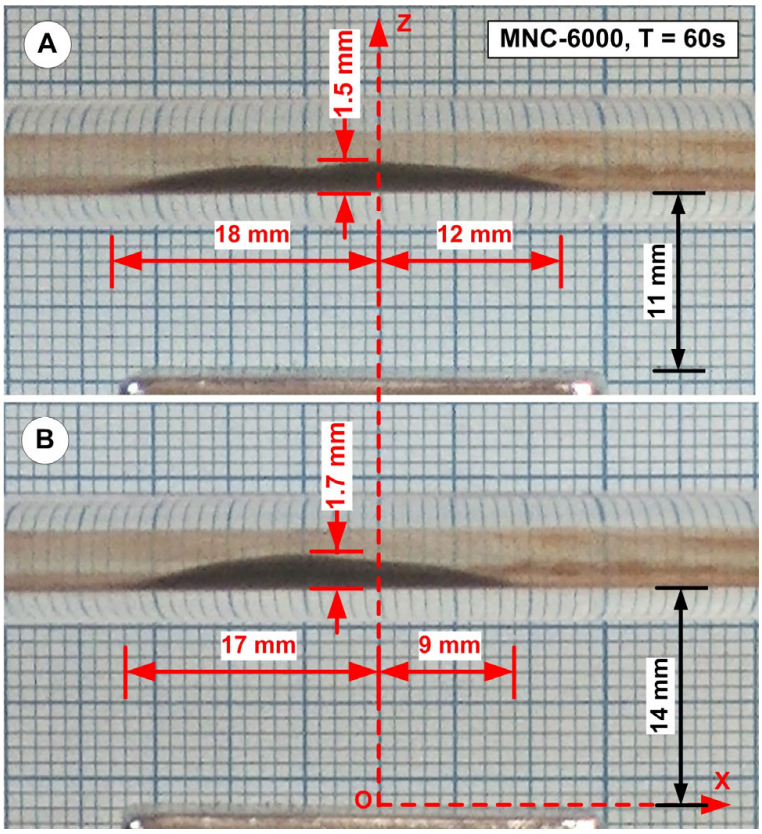


Figure 18. Influence of magnet distance on MNC-6000 retention. (**A**) Magnet distance of 11 mm and (**B**) magnet distance of 14 mm. In both cases, we have pulsatile flow, the same magnet (NbFeB52) (dimensions 30 × 20 × 20), a T = 60 s injection period, and 50 mg of injected MNCs (MNC-6000).

4.3. Influence of Magnet Distance

The strength of the magnetic field increases as the distance between the magnet and the host artery decreases (Figure 18). This results in a significantly larger concentration of MNCs in the targeted location (Table 6).

Table 6. Characteristics of particle accumulation shape along the artery lower wall at the end of the injection period of 60 s for injected MNC-6000 (quantities of 50 mg) at different magnet distances.

Magnet Distance Dt [mm]	Injected Quantity [mg]	Deposition Proximal Length L_p [mm]	Deposition Distal Length L_d [mm]	Deposition Total Length L_t [mm]	Deposition Thickness Tn [mm]	Obstruction Degree [%]	Magnet Coverage Degree [%]	Proximal Deposition Degree [%]
11	50	12	18	30	1.5	50	100	40
14		9	17	26	1.7	56.7	86.7	34.6

The buildup of MNPs during magnetic targeting narrows the local flow space, increasing fluid velocity and the corresponding hydrodynamic drag force. This finding is consistent with our previous results [40,41].

The size of particles considerably impacts capturing efficiency due to the interplay between drag and magnetic force. The drag force exerted on particles is proportional to their diameter. Furthermore, the magnetic force is proportional to the particle diameter's third power (cubic). As particle size rises, we predict that magnetic force will surpass drag

force, increasing capture efficiency. Figure 18 depicts this impact in our circumstances, where the nanocluster diameter is around 90 nm (for MNC-6000, see Figure 5).

Figure 18 and Table 6 show that a stronger magnetic field (linked to a shorter magnet distance) increased the degree of vessel obstruction by 13.2% (from 50% for Dt = 11 mm to 56.6% for Dt = 14 mm) and decreased magnet coverage by 13.3% (from 100% for Dt = 11 mm to 867% for Dt = 14 mm). Also, it reduced the degree of proximal deposition by 8.5% (from 40% for Dt = 11 mm to 36.6% for Dt = 14 mm).

Figure 19 rigorously examines the impact of magnet distance (in terms of produced magnetic force) on the given efficiency parameters.

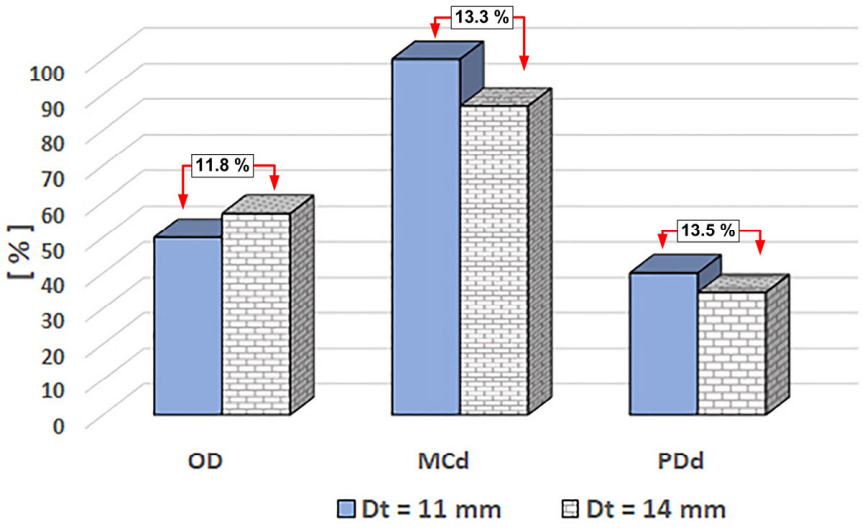


Figure 19. Magnet distance impacts the defined efficiency parameters for MNC-6000. The efficiency parameter value is given in per cent [%]. The comparisons (in percent) reflect the difference compared to the value corresponding to the magnet distance of 11 mm. Dt [mm] represents the magnet distance from the vessel's lower wall. All measurements were performed under the same conditions: MCN-6000 mass concentration of 0.5%, pulsatile flow, injection period of T = 60 s, and the same magnet (NbFeB52).

With increasing magnet distance, the shape of the deposit undergoes significant changes. This is accompanied by a noticeable increase in the degree of flow section obturation, from 50% to 56.7%, corresponding to magnet distances Dt of 11 and 14 mm. This substantial occlusion leads to a reconfiguration of the flow structure near the deposition site, resulting in the formation of two distinct flow zones and the emergence of a recirculation zone immediately beyond the deposition. These flow zones are characterized by an acceleration zone, where the hydrodynamic force dominates the magnetic force, and a flow deceleration zone in the second section of the flow. This section is particularly important as it influences the shape of the deposition, which is determined by the pulsatile flow regime, the magnetic force generated in this area, and the magnetization of the clusters present in the flow section.

As the magnetic field drops, the deposition length is reduced from 100% coverage for a Dt of 11 mm to 86.7% for a Dt of 14 mm. This drop is connected to a decrease in proximal deposition due to the action of the hydrodynamic force. It is worth mentioning that the emergence of a recirculation zone correlated with the pulsatile flow caused the deposition to take the shape of a hill. This recirculation zone creates a flow stagnation region with increased particle residence time, resulting in a higher absorption of magnetic particles distal to the deposition.

The strength of this recirculation zone is directly proportional to the pulsation frequency, with a higher intensity in the systolic phase and a lower intensity in the diastolic phase (the flow phase is presented in Figure 13).

Changing the magnet distance results in the same deposit generation mechanism for all types of MNCs studied. It is crucial to note that, despite the consistency in the deposit shape generation, variations in the coating agent's molar weight have a visible influence on the established efficiency parameters (Figure S4, Table S1, and Figure S5 in the Supplementary Files).

4.4. Influence of the Injection Period

Obtaining favourable organ distribution for a specific nanodevice remains difficult in nano delivery. This difficulty is mainly related to the duration of drug particle injection.

Using stated efficiency factors, this section investigates the influence of injection time on capturing efficiency. As a result, in this work, we varied the period of nanofluid injection between 40, 50, and 60 s (Table 7 and Figure 20).

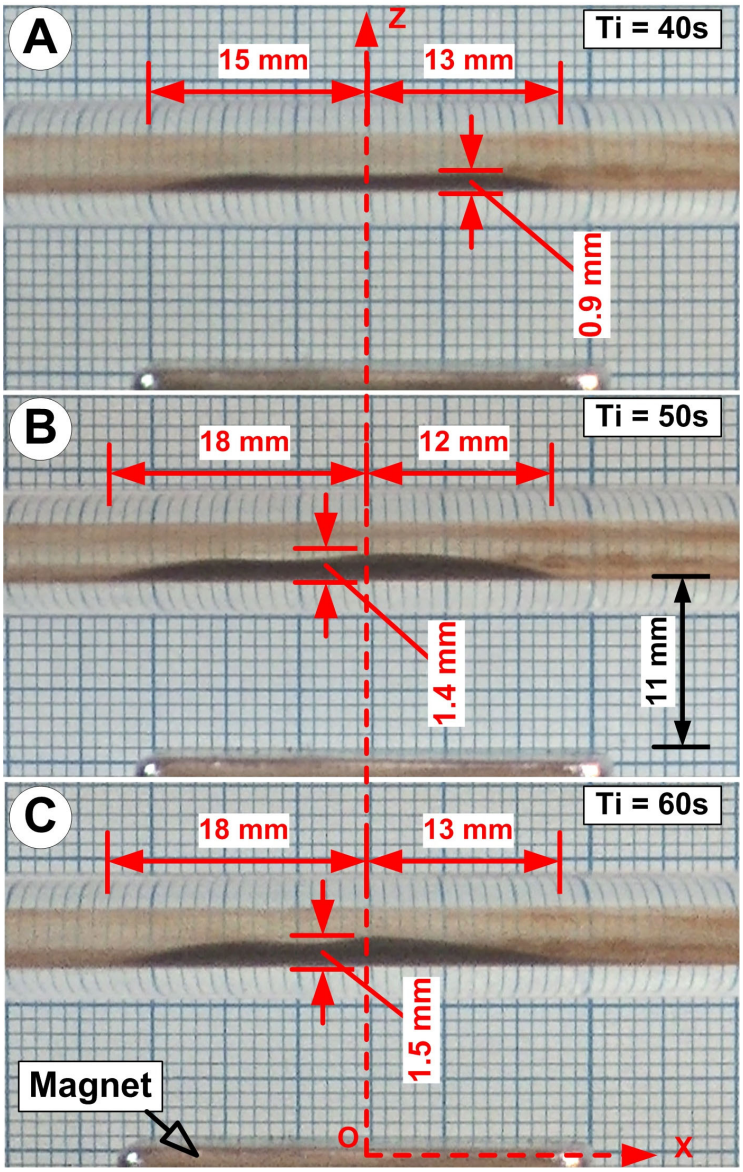


Figure 20. The influence of injection time on the cluster's deposition shape for MNC-6000: (**A**) 40 s; (**B**) 50 s; (**C**) 60 s. Ti = injection time [s]. The figure shows the MNC deposition geometric characteristics: total deposition length, the maximum deposition thickness, and proximal and distal deposition length. We use pulsatile flow, the same magnet (NbFeB52), and 50 mg of injected MNC-6000 for all cases.

Table 7. Characteristics of particle accumulation shape along the artery lower wall at the end of the different injection periods for injected MNC-6000 (quantities of 50 mg) for the same magnet distance of 11 mm.

Injection Period T [s]	Magnet Distance Dt [mm]	Injected Quantity [mg]	Deposition Proximal Length L_p [mm]	Deposition Distal Length L_d [mm]	Deposition Total Length L_t [mm]	Deposition Thick-ness Tn [mm]	Obstruction Degree [%]	Magnet Coverage Degree [%]	Proximal Deposition Degree [%]
40	11	50	13	15	28	0.9	30	93.3	46.3
50			12	18	30	1.4	46.7	100	40
60			13	18	31	1.5	50	103.3	42

As seen in Figure 20, the suspension injection time determines the morphology of the deposited MNC-6000.

The injection time considerably influences the MNC deposition morphologies of all examined nanocluster kinds (Figure S6 and Table S2 in the Supplementary Files).

Figure 21 quantitatively examines the influence of injection time on efficiency measures. Thus, it is discovered that the degree of blockage of the flow section in the deposition region is dependent on the injection time, with the degree of blockage rising from 30% for the injection time of 40 s to 46.7% and 50% for the injection times of 50 s and 60 s. We discovered that prolonging the injection period to 50 or 60 s increases the degree of obturation by 55.6% or 66.7%, respectively, compared to the injection interval of 40 s.

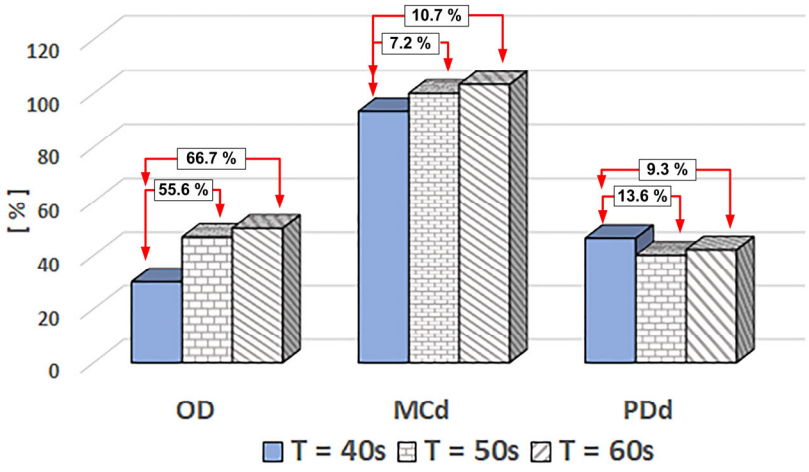


Figure 21. Injection time impacts the efficiency parameters of MNC-6000. The efficiency parameter value is given in percent [%]. The comparisons (in percent) reflect the difference compared to the value corresponding to the injection time of 40 s. T [s]—represents the injection period. All measurements were performed in the same conditions: MCN-6000 mass concentration was 0.5%, pulsatile flow, and the same magnet (NbFeB52).

The magnet's degree of coverage exhibits a complex pattern as the injection duration increases, peaking at approximately 11% for a 60-s injection. When we correlate the magnet's degree of coverage with the proximal segment's degree of coverage, we uncover the intricate effect of pulsating flow. This flow induces the transport of many clusters upstream of the area of interest, propelled by a flow force that surpasses the magnetic force upon entering the magnet's area of action. A fraction of these clusters, carried by the fluid current, are trapped in the second segment of the magnet, leading to deposition, while the majority are flushed downstream in the test circuit.

The other two suspensions (MNC-2000 and MNC-10,000) exhibit similar behaviour, as demonstrated in Figure S7 (in Supplementary File). The clusters functionalized with PEG2000 show a relatively homogeneous deposition over the length of the magnet. This

reasonably homogeneous distribution is distinguished by a modest level of obturation, with values ranging from 23.3% to 26.7% for injection periods of 40 s and 60 s, respectively. It is also worth noting that the degree of magnet coverage is almost complete for each injection period, and the degree of proximal coverage is considerable, with values ranging from 53.8% to 31.3% for injection times of 40 s and 60 s, respectively.

5. Limitations

A variety of uncertainty factors contributed to the heterogeneity of the cluster deposition morphologies. Unfortunately, it is impossible to separate this effect from other sources of error in the experiment, such as particles becoming stuck in the injection mechanism, particles clumping together and falling to the bottom of the tube before entering the test section, particles clinging to the tube's wall before reaching the desired section, or the position of the needle during injection. Despite the regrettable inability to eliminate or control the causes of error in the experiment, it is critical to note that a true magnetic drug-targeting therapy would have all these faults.

In our work, camera images were taken during measurements and used to extract MNC distributions and depositions. This represents another source of error regarding the deposition morphology investigations.

Human arteries are convoluted, and artery walls are not flat. It is critical to recognize that particles may cling to artery walls, like in the current experimental setup, and induce differences in the particle's quantities deposited in the desired artery segments. When designing a magnetic medication therapy, it is critical to consider this impact and account for any inaccuracies. It is important to note that our current experimental vessels, while valuable for initial studies, may not fully replicate the complexities of natural vessels. Because the distance between the magnet and the vessel is inconsistent in natural 3D geometries, particle dispersion and form deposition may differ from the results presented in this paper.

Furthermore, in real life, particles are injected into the artery slowly over many minutes via a catheter [58], but in this investigation, all particles were released in 40 to 60 s.

The literature describes the importance of magnetic particle-release positions, especially the needle position in the artery cross-section (either in the artery core or near the artery wall) [4]. In our experiments, we injected the MNC dispersion roughly into the vessel's centre.

6. Considerations Regarding Particle-Targeting Applications and Medical Implications

Many studies have been conducted on preventing particle entrapment, often by installing two or more magnets or electromagnets on opposite sides of a vessel [59–61]. While this approach can be practical in a controlled laboratory setting, it is not feasible for real MDT therapy in the human body. Therefore, a practical consensus is forming among researchers [40,62,63], including those in our study, in favour of particle guidance using a permanent magnet positioned on one side of the target vessel. This approach effectively addresses the limitations of multiple magnets on opposite sides and highlights the advantages of placing the magnet on only one side of the target vessel.

Given the practical considerations in medical applications, using multiple magnets around the vessel is not viable. Therefore, our research is centred on the use of a single permanent magnet. Due to employing ordinary magnets (commercially available permanent magnets) in our study, various factors, such as the magnet's geometric form and magnetism, influence the shape and position of MNC deposition.

Magnetic particle cores with well-defined and reproducible structural, physical, chemical, and pharmacological properties are needed for biomedical applications.

Based on our findings, we believe the following requirements must be included in their elaboration: (i) An excellent response to an applied magnetic field is crucial as it ensures efficient and precise control over the particles in biomedical applications. (ii) Particles with negligible remanence, meaning they retain little-to-no magnetization after the external

field is turned off, are essential. This property ensures minimal or no magnetic interactions and agglomeration, enhancing the particles' performance in biomedical applications. (iii) Another crucial requirement is a well-defined size and level of monodispersity. We also propose using the smallest size possible, as smaller particles offer larger total surface areas for functionalization, enhancing their biomedical applications.

In general, the literature defines the "targeting efficiency" parameter as a qualitative classification criterion of the targeting process, defined as the ratio of the amount or number of injected particles to the quantity or number of particles caught in the region of interest.

Targeted drug delivery causes a large amount of medications to be lost in the circulation, so it does not significantly help to repair the damaged arterial segment. Our fundamental notion is that magnetic clusters circulate freely throughout the circulatory system and may be readily steered to the appropriate artery segment using an external magnetic field.

More importantly, we believe that depositing a thin layer of medication, uniformly covering the vascular wall in the area of interest is the only way to achieve maximum efficiency in targeted drug delivery. This ensures the proper contact of the nanocarrier's surface with the vascular wall, adequate absorption of the medicine, and the delivery of the appropriate dosage during the treatment. In the specific case of magnetic drug targeting, the shape of the depositions is a result of the intricate competition between the magnetic and hydrodynamic forces, underscoring the complexity of this drug-targeting technique.

Based on this need, we have created a set of efficiency criteria in this study, with more explicit definitions, to emphasise the critical parts of the targeting process. Consequently, we have established the following efficiency parameters:

1. Obstruction degree (OD) measures the highest decrease in arterial cross-section following particle deposition. The obstruction degree (OD) is a critical efficiency measure, showing that a higher degree of occlusion leads to lower deposition efficiency since the deposition is concentrated in a smaller area than is required. In the first step, we established a threshold of 20% blockage of the studied artery's diameter.
2. Another critical efficiency parameter we have established is the magnet coverage degree (MCd). This measure plays a significant role in determining the quality of deposition, as it considers the length of the magnet. The closer the coverage is to 100%, the more uniform the particle deposition. This indicates that the chosen magnet effectively captures particles in the desired location and along the entire length of the damaged artery.
3. Proximal deposition degree (PDd): measures the effect of pulsatile flow on the deposition length considering the magnet's length in relation to the targeted region's entry section. The closer this ratio is to 50% (equivalent to half of the magnet's length), the more uniform the deposition. This suggests that the magnet utilized creates a strong enough magnetic force to balance the hydrodynamic force.

Our experiments examined three distinct water-based solutions, each including a PEG-coated cluster with a varying molecular weight (2000 Da, 6000 Da, and 10,000 Da). The dispersion condition of all PEG Mw-coated particles was analysed using transmission electron microscopy (TEM), while the number and intensity density distribution of individual particles or agglomerates were assessed by DLS examination. The impact of PEG Mw may be linked to alterations in the clusters' dispersion states, whether in an individual or agglomerated form.

Scientists have shown that the dimensions and morphology of nanoparticles (NPs) play a crucial role in regulating how long they circulate in the bloodstream and how well they adhere to the walls of blood vessels. The margination propensity of nanoparticles (NPs) in the blood is determined by their size, shape, surface characteristics, and stiffness, referred to as the '4S' factors in [64].

Thus, the margining of particles in the blood flow allows them to pass through the leaky artery wall under the EPR effect at the cancer's location. Ye [64] claims that bigger particles are more likely to gather in the near-wall area.

Conversely, Qiu et al. [7] demonstrated that an external magnetic field can enhance the permeability of the vascular endothelium. Their research confirms that an external magnetic field can effectively regulate the permeability of the vascular endothelium without impairing its functions. Furthermore, Qiu's [7] and Alavijeh's [65] work underscores that the localization of particles depends on the vascular wall's diffusive permeability. According to these studies, the largest size of nanoparticles that can pass through human cell membranes is around 1 µm. The choice of particle size for targeting applications is directly linked to specific targeting objectives, such as targeting atherosclerotic artery segments, cancer cells, or medical devices like stents, or delivering specific cargo.

Despite the larger size of the investigated particles, which had a hydrodynamic diameter of around 550 nm, and considering the findings presented by Qiu [7] and Alavijeh [65], we believe that further research could make them a viable candidate for use in medical applications, such as share-induced particle deposition.

7. Next Steps

Considering the several restrictions and findings of this investigation, we must carry out the following actions in the future to improve the effectiveness of these kinds of clusters:

1. In our experiments, we injected the MNC dispersion roughly into the vessel's centre. In our future studies, we will investigate the impact of injection position (distance from the targeted region and needle position regarding the vessel centre) on the stated efficiency characteristics.
2. In our subsequent studies, we plan to expand our research to include a wider variety of magnet types. This will allow us to understand the relationship between the established deposition efficiency parameters and the magnetic fields generated by these magnets, with direct implications for the practical application of our findings.
3. We also propose the use of nanoclusters with a smaller size. Smaller particles have more extensive overall surface areas for functionalization, which improves their biological uses. Specifically, we will alter the solvothermal polyol method to produce nanoclusters with hydrodynamic diameters as tiny as possible (less than 500 nm).
4. To replicate the actual medical setting of drug delivery as closely as possible, we want to increase the injection duration to the order of minutes.

8. Conclusions

In the present study, we evaluated the magnetic accumulation of three types of MNCs coating agents of different molecular weights (Mw), namely, (i) MNC-2000, which has an Mw of 2000 Da, a TEM measured size of 67 nm, and a hydrodynamic diameter of 628 nm; (ii) MNC-6000, which has an Mw of 6000 Da, a TEM measured size of 89 nm, and a hydrodynamic diameter of 535 nm; and MNC-10,000, which has an Mw of 10,000 Da, a TEM measured size of 80 nm, and a hydrodynamic diameter of 579 nm.

The considerable differences in the used PEG molecular weights to coat the magnetite nanoclusters resulted in differences in their magnetic accumulation under flow conditions, Our key findings are as follows:

1. Our study underscores a key finding: the distance between the magnetic field source and vessels played a crucial role in particle steering, regardless of the molar weight of the PEG used, in all investigated MNCs.
2. In actual MDT therapy, approximately 10^{10} particles per mL [66] with injection volumes of approximately 5 mL to 10 mL [55,67,68] are injected into the patient. We injected 10 mL suspensions containing MNCs with 0.4% and 0.5% mass concentrations in our experiments. This concentration is lower than the maximum human-safe dose of the cancer drug doxorubicin used in clinical practice. Our experiments have revealed that these clusters may target medications even under these settings. The utilized amounts of MNCs also demonstrate how molar weight influences deposition efficiency in the presence of external magnetic fields.

3. Furthermore, the experiments with varying quantities of injected material demonstrated that using 50 mg of clusters results in much higher efficiency metrics than using 40 mg of clusters, independent of the molar mass of the PEG utilized.
4. The pulsatile character of the flow, regardless of the molar mass of the coating agent utilized, determines the shape and effectiveness of cluster deposition in the region of interest. It is crucial to note that the use of a pulsatile flow signal to reproduce a natural cardiovascular flow regime with a high degree of fidelity not only highlights the influence of the acceleration and deceleration phases on the deposition morphology but also underscores the necessity of a pulsating flow to obtain specific results with high confidence in magnetic targeting applications.
5. The presence of particle deposition, especially depositions with a high degree of occlusion in the artery section, induces a change in the blood's behaviour in the vicinity of the deposition. This change is due to the recirculation zone's development and presence in the deposition's distal part, as presented in Section 4.3. Regardless of the PEG's molar mass, this aspect becomes apparent as the magnet's distance from the area of interest changes and is present for practically all investigated clusters. During the investigations on the influence of magnet distance, this phenomenon most strongly manifested itself for the MNC-6000 clusters, followed by the MNC-2000 clusters.
6. To assess the impact of injection time on deposition efficiency metrics, we aimed to evaluate the effect of PEG molar weight on deposition uniformity. The analysed injection periods of 40, 50, and 60 s indicated that MNC-2000 received the best certification for all efficiency metrics, followed by MNC-10,000 and MNC-6000, in that order.

Based on the analysis of the results obtained for all three types of investigated clusters, we can conclude that MNC-2000-type clusters ensure maximum deposition efficiency, followed by MNC-6000 and MNC-10,000 clusters. Although the efficiency parameters of the MNC-6000 and MNC-10,000 clusters differ, we can differentiate their efficiency by analysing the specific requirements of each application.

To sum up, the targeting process for particles made and modified through the solvothermal synthesis process is greatly affected by the increase in the molar mass of the coating agent (PEG, in this case).

Supplementary Materials: The following supporting information can be downloaded at: https://www.mdpi.com/article/10.3390/magnetochemistry10070051/s1, Supplementary File: Deposition efficiency investigation, Video S1: Deposition shape formations during MNC-6000 magnetic targeting.

Author Contributions: Conceptualization, writing—original draft, writing—review and editing, visualization, investigation, S.I.B. and A.B.; conceptualization, investigation, R.T. and V.S.; methodology, validation, S.I.B., V.S., A.B., R.T., M.C.I. and E.S.B.; investigation, validation, R.T., M.D., M.C.I., D.S.-R. and E.S.B. All authors have read and agreed to the published version of the manuscript.

Funding: This research received no external funding.

Institutional Review Board Statement: Not applicable.

Informed Consent Statement: Not applicable.

Data Availability Statement: Data are contained within the article and Supplementary Materials.

Acknowledgments: For S.I. Bernad, this work was supported by the RA-TB/CFATR/LHC multiannual research program 2023–2024. For V. Socoliuc, this work was supported partially by the RA-TB/CFATR/LMF multiannual research program 2023–2024 and a grant from the Ministry of Research, Innovation and Digitization, CNCS/CCCDI—UEFISCDI, project number PN-III P2-2.1-PED-2021-2049, within PNCDI III. For A. Bunge, M. Ioncica, R. Turcu, and E. Bernad, this work was supported partially by a grant from the Ministry of Research, Innovation and Digitization, CNCS/CCCDI—UEFISCDI, project number PN-III-P2-2.1-PED-2021-2049, within PNCDI III.

Conflicts of Interest: The authors declare no conflicts of interest.

References

1. Lindstrom, M.; DeCleene, N.; Dorsey, H.; Fuster, V.; Johnson, C.O.; LeGrand, K.E.; Mensah, G.A.; Razo, C.; Stark, B.; Turco, J.V.; et al. Global Burden of Cardiovascular Diseases and Risks Collaboration, 1990–2021. *J. Am. Coll. Cardiol.* **2022**, *80*, 2372–2425. [CrossRef] [PubMed]
2. World Heart Report 2023: Confronting the World's Number One Killer. 2023. Available online: https://heartreport23.world-heart-federation.org (accessed on 2 April 2024).
3. Naghavi, M.; Libby, P.; Falk, E.; Casscells, S.W.; Litovsky, S.; Rumberger, J.; Badimon, J.J.; Stefanadis, C.; Moreno, P.; Pasterkamp, G.; et al. From Vulnerable Plaque to Vulnerable Patient: A Call for New Definitions and Risk Assessment Strategies: Part I. *Circulation* **2003**, *108*, 1664–1672. [CrossRef] [PubMed]
4. Manshadi, M.K.D.; Saadat, M.; Mohammadi, M.; Shamsi, M.; Dejam, M.; Kamali, R.; Sanati-Nezhad, A. Delivery of magnetic micro/nanoparticles and magnetic-based drug/cargo into arterial flow for targeted therapy. *Drug Deliv.* **2018**, *25*, 1963–1973. [CrossRef]
5. Tibbitt, M.W.; Dahlman, J.E.; Langer, R. Emerging Frontiers in Drug Delivery. *J. Am. Chem. Soc.* **2016**, *138*, 704–717. [CrossRef] [PubMed]
6. Maeda, H.; Nakamura, H.; Fang, J. The EPR effect for macromolecular drug delivery to solid tumors: Improvement of tumor uptake, lowering of systemic toxicity, and distinct tumor imaging in vivo. *Adv. Drug Deliv. Rev.* **2013**, *65*, 71–79. [CrossRef] [PubMed]
7. Qiu, Y.; Tong, S.; Zhang, L.; Sakurai, Y.; Myers, D.R.; Hong, L.; Lam, W.A.; Bao, G. Magnetic forces enable controlled drug delivery by disrupting endothelial cell-cell junctions. *Nat. Commun.* **2017**, *8*, 15594. [CrossRef] [PubMed]
8. Kostopoulou, A.; Lappas, A. Colloidal magnetic nanocrystal clusters: Variable length-scale interaction mechanisms, synergetic functionalities and technological advantages. *Nanotechnol. Rev.* **2015**, *4*, 595–624. [CrossRef]
9. Wang, Q.; Ma, X.; Liao, H.; Liang, Z.; Li, F.; Tian, J.; Ling, D. Artificially Engineered Cubic Iron Oxide Nanoparticle as a High-Performance Magnetic Particle Imaging Tracer for Stem Cell Tracking. *ACS Nano* **2020**, *14*, 2053–2062. [CrossRef]
10. de Montferrand, C.; Hu, L.; Milosevic, I.; Russier, V.; Bonnin, D.; Motte, L.; Brioude, A.; Lalatonne, Y. Iron oxide nanoparticles with sizes, shapes and compositions resulting in different magnetization signatures as potential labels for multiparametric detection. *Acta Biomater.* **2013**, *9*, 6150–6157. [CrossRef]
11. Zamani Kouhpanji, M.R.; Stadler, B.J.H. A Guideline for Effectively Synthesizing and Characterizing Magnetic Nanoparticles for Advancing Nanobiotechnology: A Review. *Sensors* **2020**, *20*, 2554. [CrossRef]
12. Kostopoulou, A.; Tsiaoussis, I.; Lappas, A. Magnetic iron oxide nanoclusters with tunable optical response. *Photonics Nanostructures-Fundam. Appl.* **2011**, *9*, 201–206. [CrossRef]
13. Holmlin, R.E.; Chen, X.; Chapman, R.G.; Takayama, S.; Whitesides, G.M. Zwitterionic SAMs that Resist Nonspecific Adsorption of Protein from Aqueous Buffer. *Langmuir* **2001**, *17*, 2841–2850. [CrossRef] [PubMed]
14. Pillai, P.P.; Huda, S.; Kowalczyk, B.; Grzybowski, B.A. Controlled pH Stability and Adjustable Cellular Uptake of Mixed-Charge Nanoparticles. *J. Am. Chem. Soc.* **2013**, *135*, 6392–6395. [CrossRef] [PubMed]
15. Gref, R.; Minamitake, Y.; Peracchia, M.; Trubetskoy, V.; Torchilin, V.; Langer, R. Biodegradable long-circulating polymeric nanospheres. *Science* **1994**, *263*, 1600–1603. [CrossRef] [PubMed]
16. Hu, C.-M.J.; Fang, R.H.; Luk, B.T.; Zhang, L. Polymeric nanotherapeutics: Clinical development and advances in stealth functionalization strategies. *Nanoscale* **2014**, *6*, 65–75. [CrossRef] [PubMed]
17. Guerrini, L.; Alvarez-Puebla, R.; Pazos-Perez, N. Surface Modifications of Nanoparticles for Stability in Biological Fluids. *Materials* **2018**, *11*, 1154. [CrossRef] [PubMed]
18. Li, S.-D.; Huang, L. Stealth nanoparticles: High density but sheddable PEG is a key for tumor targeting. *J. Control. Release* **2010**, *145*, 178–181. [CrossRef] [PubMed]
19. Hong, L.; Wang, Z.; Wei, X.; Shi, J.; Li, C. Antibodies against polyethylene glycol in human blood: A literature review. *J. Pharmacol. Toxicol. Methods* **2020**, *102*, 106678. [CrossRef]
20. Ben-Shabat, S.; Kumar, N.; Domb, A.J. PEG-PLA Block Copolymer as Potential Drug Carrier: Preparation and Characterization. *Macromol. Biosci.* **2006**, *6*, 1019–1025. [CrossRef]
21. Fang, C.; Shi, B.; Pei, Y.-Y.; Hong, M.-H.; Wu, J.; Chen, H.-Z. In vivo tumor targeting of tumor necrosis factor-α-loaded stealth nanoparticles: Effect of MePEG molecular weight and particle size. *Eur. J. Pharm. Sci.* **2006**, *27*, 27–36. [CrossRef]
22. Chen, B.-M.; Cheng, T.-L.; Roffler, S.R. Polyethylene glycol immunogenicity: Theoretical, clinical, and practical aspects of anti-polyethylene glycol antibodies. *ACS Nano* **2021**, *15*, 14022–14048. [CrossRef] [PubMed]
23. Shi, D.; Beasock, D.; Fessler, A.; Szebeni, J.; Ljubimova, J.Y.; Afonin, K.A.; Dobrovolskaia, M.A. To PEGylate or not to PEGylate: Immunological properties of nanomedicine's most popular component, poly (ethylene) glycol and its alternatives. *Adv. Drug Deliv. Rev.* **2021**, *180*, 114079. [CrossRef] [PubMed]
24. Shimizu, T.; Mima, Y.; Hashimoto, Y.; Ukawa, M.; Ando, H.; Kiwada, H.; Ishida, T. Anti-PEG IgM and complement system are required for the association of second doses of PEGylated liposomes with splenic marginal zone B cells. *Immunobiology* **2015**, *220*, 1151–1160. [CrossRef] [PubMed]
25. Emam, S.E.; Elsadek, N.E.; Abu Lila, A.S.; Takata, H.; Kawaguchi, Y.; Shimizu, T.; Ando, H.; Ishima, Y.; Ishida, T. Anti-PEG IgM production and accelerated blood clearance phenomenon after the administration of PEGylated exosomes in mice. *J. Control. Release* **2021**, *334*, 327–334. [CrossRef] [PubMed]

26. Stone, C.A., Jr.; Liu, Y.; Relling, M.V.; Krantz, M.S.; Pratt, A.L.; Abreo, A.; Hemler, J.A.; Phillips, E.J. Immediate hypersensitivity to polyethylene glycols and polysorbates: More common than we have recognized. *J. Allergy Clin. Immunol. Pract.* **2019**, *7*, 1533–1540.e8. [CrossRef] [PubMed]
27. Szebeni, J.; Simberg, D.; González-Fernández, Á.; Barenholz, Y.; Dobrovolskaia, M.A. Roadmap and strategy for overcoming infusion reactions to nanomedicines. *Nat. Nanotechnol.* **2018**, *13*, 1100–1108. [CrossRef] [PubMed]
28. Xiao, Z.; Zhang, L.; Colvin, V.L.; Zhang, Q.; Bao, G. Synthesis and Application of Magnetic Nanocrystal Clusters. *Ind. Eng. Chem. Res.* **2022**, *61*, 7613–7625. [CrossRef]
29. Xu, X.; Xiang, H.; Wang, Z.; Wu, C.; Lu, C. Doping engineering and functionalization of iron oxide nanoclusters for biomedical applications. *J. Alloys Compd.* **2022**, *923*, 166459. [CrossRef]
30. Craciunescu, I.; Petran, A.; Liebscher, J.; Vekas, L.; Turcu, R. Synthesis and characterization of size-controlled magnetic clusters functionalized with polymer layer for wastewater depollution. *Materials Chem. Phys.* **2017**, *185*, 91–97. [CrossRef]
31. Fiévet, F.; Brayner, R. The Polyol Process. In *Nanomaterials: A Danger or a Promise? A Chemical and Biological Perspective*; Brayner, R., Fiévet, F., Coradin, T., Eds.; Springer: London, UK, 2013; pp. 1–25.
32. Deng, H.; Li, X.L.; Peng, Q.; Wang, X.; Chen, J.P.; Li, Y.D. Monodisperse magnetic single-crystal ferrite microspheres. *Angew. Chem. Int. Ed.* **2005**, *44*, 2782–2785. [CrossRef]
33. Bunge, A.; Leoștean, C.; Radu, T.; Tripon, S.C.; Borodi, G.; Turcu, R. Substituted Poly(Vinylphosphonate) Coatings of Magnetite Nanoparticles and Clusters. *Magnetochemistry* **2022**, *8*, 79. [CrossRef]
34. Susan-Resiga, D.; Socoliuc, V.; Bunge, A.; Turcu, R.; Vékás, L. From high colloidal stability ferrofluids to magnetorheological fluids: Tuning the flow behavior by magnetite nanoclusters. *Smart Mater. Struct.* **2019**, *28*, 115014. [CrossRef]
35. Rafienia, M.; Bigham, A.; Hassanzadeh-Tabrizi, S.A. Solvothermal Synthesis of Magnetic Spinel Ferrites. *J. Med. Signals Sens.* **2018**, *8*, 108–118. [CrossRef]
36. Xuan, S.H.; Wang, Y.X.J.; Yu, J.C.; Leung, K.C.F. Tuning the Grain Size and Particle Size of Superparamagnetic Fe_3O_4 Microparticles. *Chem. Mater.* **2009**, *21*, 5079–5087. [CrossRef]
37. Ge, J.P.; Hu, Y.X.; Biasini, M.; Beyermann, W.P.; Yin, Y.D. Superparamagnetic magnetite colloidal nanocrystal clusters. *Angew. Chem. Int. Ed.* **2007**, *46*, 4342–4345. [CrossRef] [PubMed]
38. Bunge, A.; Porav, A.S.; Borodi, G.; Radu, T.; Pirnau, A.; Berghian-Grosan, C.; Turcu, R. Correlation between synthesis parameters and properties of magnetite clusters prepared by solvothermal polyol method. *J. Mater. Sci.* **2019**, *54*, 2853–2875. [CrossRef]
39. Liu, J.; Lv, Y.; Zhang, W.; Zhang, Z.; Wang, A. Tailoring the structural and optical properties of RF magnetron sputtered ZnO/graphene thin films by annealing temperature. *Integr. Ferroelectr.* **2019**, *198*, 142–152. [CrossRef]
40. Bernad, S.I.; Bernad, E. Magnetic Forces by Permanent Magnets to Manipulate Magnetoresponsive Particles in Drug-Targeting Applications. *Micromachines* **2022**, *13*, 1818. [CrossRef] [PubMed]
41. Bernad, S.I.; Susan-Resiga, D.; Bernad, E. Hemodynamic Effects on Particle Targeting in the Arterial Bifurcation for Different Magnet Positions. *Molecules* **2019**, *24*, 2509. [CrossRef]
42. Cregg, P.J.; Murphy, K.; Mardinoglu, A. Inclusion of interactions in mathematical modelling of implant assisted magnetic drug targeting. *Appl. Math. Model.* **2012**, *36*, 1–34. [CrossRef]
43. Camacho, J.M.; Sosa, V. Alternative method to calculate the magnetic field of permanent magnets with azimuthal symmetry. *Rev. Mex. Fis.* **2013**, *59*, 8–17.
44. Bernad, S.I.; Socoliuc, V.; Susan-Resiga, D.; Crăciunescu, I.; Turcu, R.; Tombácz, E.; Vékás, L.; Ioncica, M.C.; Bernad, E.S. Magnetoresponsive Functionalized Nanocomposite Aggregation Kinetics and Chain Formation at the Targeted Site during Magnetic Targeting. *Pharmaceutics* **2022**, *14*, 1923. [CrossRef] [PubMed]
45. Bernad, S.I.; Craciunescu, I.; Sandhu, G.S.; Dragomir-Daescu, D.; Tombacz, E.; Vekas, L.; Turcu, R. Fluid Targeted delivery of functionalized magnetoresponsive nanocomposite particles to a ferromagnetic stent. *J. Magn. Magn. Mater.* **2021**, *519*, 167489. [CrossRef]
46. Hu, L.; Percheron, A.; Chaumont, D.; Brachais, C.-H. Microwave-assisted one-step hydrothermal synthesis of pure iron oxide nanoparticles: Magnetite, maghemite and hematite. *J. Sol-Gel Sci. Technol.* **2011**, *60*, 198. [CrossRef]
47. Silva, M.G.d.; Santiago, L.E.P.; Fernandes, R.d.S.; Padilha, C.E.d.A.; Souza, D.F.d.S. Analysis of thermal decomposition of magnetic nanoparticles synthesized by reverse coprecipitation and partial oxidation of ferrous ions. *Braz. J. Chem. Eng.* **2023**, *41*, 347–357. [CrossRef]
48. García-Jimeno, S.; Estelrich, J. Ferrofluid based on polyethylene glycol-coated iron oxide nanoparticles: Characterization and properties. *Colloids Surf. A Physicochem. Eng. Asp.* **2013**, *420*, 74–81. [CrossRef]
49. Zhong, Z.; Chen, F.; Subramanian, A.S.; Lin, J.; Highfield, J.; Gedanken, A. Assembly of Au colloids into linear and spherical aggregates and effect of ultrasound irradiation on structure. *J. Mater. Chem.* **2006**, *16*, 489–495. [CrossRef]
50. Malabanan, J.W.T.; Alcantara, K.P.; Jantaratana, P.; Pan, Y.; Nalinratana, N.; Vajragupta, O.; Rojsitthisak, P.; Rojsitthisak, P. Enhancing Physicochemical Properties and Biocompatibility of Hollow Porous Iron Oxide Nanoparticles through Polymer-Based Surface Modifications. *ACS Appl. Bio Mater.* **2023**, *6*, 5426–5441. [CrossRef]
51. Alexis, F.; Pridgen, E.; Molnar, L.K.; Farokhzad, O.C. Factors Affecting the Clearance and Biodistribution of Polymeric Nanoparticles. *Mol. Pharm.* **2008**, *5*, 505–515. [CrossRef]
52. Carreau, P.J. Rheological Equations from Molecular Network Theories. *Trans. Soc. Rheol.* **1972**, *16*, 99–127. [CrossRef]

53. Kumar, S.R.; Marianna, L.; Gianni, S.; Nathanael, A.J.; Hong, S.I.; Hwan Oh, T.; Mangalaraj, D.; Viswanathan, C.; Ponpandian, N. Hydrophilic polymer coated monodispersed Fe_3O_4 nanostructures and their cytotoxicity. *Mater. Res. Express* **2014**, *1*, 015015. [CrossRef]
54. Luigjes, B.; Woudenberg, S.M.C.; de Groot, R.; Meeldijk, J.D.; Torres Galvis, H.M.; de Jong, K.P.; Philipse, A.P.; Erné, B.H. Diverging Geometric and Magnetic Size Distributions of Iron Oxide Nanocrystals. *J. Phys. Chem. C* **2011**, *115*, 14598–14605. [CrossRef]
55. Van Liebergen, R.A.M.; Piek, J.J.P.; Koch, K.T.; Peters, R.J.G.; de Winter, R.J.; Schotborgh, C.E.; Lie, K.I. Hyperemic coronary flow after optimized intravascular ultrasound-guided balloon angioplasty and stent implantation. *J. Am. Coll. Cardiol.* **1999**, *34*, 1899–1906. [CrossRef]
56. Chatelut, E.; White-Koning, M.L.; Mathijssen, R.H.; Puisset, F.; Baker, S.D.; Sparreboom, A. Dose banding as an alternative to body surface area-based dosing of chemotherapeutic agents. *Br. J. Cancer* **2012**, *107*, 1100–1106. [CrossRef]
57. Nacev, A.; Beni, C.; Bruno, O.; Shapiro, B. Magnetic nanoparticle transport within flowing blood and into surrounding tissue. *Nanomedicine* **2010**, *5*, 1459–1466. [CrossRef]
58. Alexiou, C.; Jurgons, R.; Schmid, R.; Bergemann, C.; Henke, J.; Erhardt, W.; Huenges, E.; Parak, F. Magnetic Drug Targeting—Biodistribution of the Magnetic Carrier and the Chemotherapeutic agent Mitoxantrone after Locoregional Cancer Treatment. *J. Drug Target.* **2003**, *11*, 139–149. [CrossRef] [PubMed]
59. Chakrabarty, P.; Paily, R.P. Time-Varying Magnetic Field to Enhance the Navigation of Magnetic Microparticles in a Bifurcated Channel. *IEEE Magn. Lett.* **2022**, *13*, 3102705. [CrossRef]
60. Durme, R.; Crevecoeur, G.; Dupré, L.; Coene, A. Improved magnetic drug targeting with maximized magnetic forces and limited particle spreading. *Med. Phys.* **2023**, *50*, 1715–1727. [CrossRef] [PubMed]
61. Abolfathi, K.; Yazdi, M.R.H.; Hoshiar, A.K. Studies of Different Swarm Modes for the MNPs Under the Rotating Magnetic Field. *IEEE Trans. Nanotechnol.* **2020**, *19*, 849–855. [CrossRef]
62. Kee, H.; Lee, H.; Park, S. Optimized Halbach array for focused magnetic drug targeting. *J. Magn. Magn. Mater.* **2020**, *514*, 167180. [CrossRef]
63. Hussain, S.; Mair, L.; Willis, A.; Papavasiliou, G.; Liu, B.; Weinberg, I.; Engelhard, H. Parallel Multichannel Assessment of Rotationally Manipulated Magnetic Nanoparticles. *Nanotechnol. Sci. Appl.* **2022**, *15*, 1–15. [CrossRef] [PubMed]
64. Ye, H.; She, Z.; Yu, L.; Wei, M.; Li, Y. Manipulating nanoparticle transport within blood flow through external forces: An exemplar of mechanics in nanomedicine. *Proc. R. Soc. A* **2018**, *474*, 20170845. [CrossRef] [PubMed]
65. Alavijeh, A.A.; Barati, M.; Barati, M.; Dehkordi, A.H. The Potential of Magnetic Nanoparticles for Diagnosis and Treatment of Cancer Based on Body Magnetic Field and Organ-on-the-Chip. *Adv. Pharm. Bull.* **2019**, *9*, 360–373. [CrossRef] [PubMed]
66. Alexiou, C.; Diehl, D.; Henninger, P.; Iro, H.; Rockelein, R.; Schmidt, W.; Weber, H. A High Field Gradient Magnet for Magnetic Drug Targeting. *IEEE Trans. Appl. Supercond.* **2006**, *16*, 1527–1530. [CrossRef]
67. Ulbrich, K.; Hola, K.; Subr, V.; Bakandritsos, A.; Tucek, J.; Zboril, R. Targeted Drug Delivery with Polymers and Magnetic Nanoparticles: Covalent and Noncovalent Approaches, Release Control, and Clinical Studies. *Chem. Rev.* **2016**, *116*, 5338–5431. [CrossRef]
68. Al-Jamal, K.T.; Bai, J.; Wang, J.T.W.; Protti, A.; Southern, P.; Bogart, L.; Heidari, H.; Li, X.; Cakebread, A.; Asker, D.; et al. Magnetic DrugTargeting: Preclinical in Vivo Studies, Mathematical Modeling, and Extrapolation to Humans. *Nano Lett.* **2016**, *16*, 5652–5660. [CrossRef]

Disclaimer/Publisher's Note: The statements, opinions and data contained in all publications are solely those of the individual author(s) and contributor(s) and not of MDPI and/or the editor(s). MDPI and/or the editor(s) disclaim responsibility for any injury to people or property resulting from any ideas, methods, instructions or products referred to in the content.